Wireless Channel Estimation and Channel Prediction for MIMO Communication Systems

by

Farnoosh Talaei
B.Sc., Isfahan University of Technology, 2008
M.Sc., Isfahan University of Technology, 2011

A Dissertation Submitted in Partial Fulfillment of the
Requirements for the Degree of

DOCTOR OF PHILOSOPHY

in the Department of Electrical and Computer Engineering

Wireless Channel Estimation and Channel Prediction for MIMO Communication Systems

by

Farnoosh Talaei
B.Sc., Isfahan University of Technology, 2008
M.Sc., Isfahan University of Technology, 2011

Supervisory Committee

Dr. Xiaodai Dong, Supervisor
(Department of Electrical and Computer Engineering)

Dr. Michael L. McGuire, Departmental Member
(Department of Electrical and Computer Engineering)

Dr. Kui Wu, Outside Member
(Department of Computer Science)

Supervisory Committee

Dr. Xiaodai Dong, Supervisor

(Department of Electrical and Computer Engineering)

Dr. Michael L. McGuire, Departmental Member

(Department of Electrical and Computer Engineering)

Dr. Kui Wu, Outside Member

(Department of Computer Science)

ABSTRACT

In this dissertation, channel estimation and channel prediction are studied for wireless communication systems. Wireless communication for time-variant channels becomes more important by the fast development of intelligent transportation systems which motivates us to propose a reduced rank channel estimator for time-variant frequency-selective high speed railway (HSR) systems and a reduced rank channel predictor for fast time-variant flat fading channels. Moreover, the potential availability of large bandwidth channels at mm-wave frequencies and the small wavelength of the mm-waves, offer the mm-wave massive multiple-input multiple-output (MIMO) communication as a promising technology for 5G cellular networks. The high fabrication cost and power consumption of the radio frequency (RF) units at mm-wave frequencies motivates us to propose a low-power hybrid channel estimator for mm-wave MIMO orthogonal frequency-division multiplexing (OFDM) systems.

The work on HSR channel estimation takes advantage of the channel's restriction to low dimensional subspaces due to the time, frequency and spatial correlation of the channel and presents a low complexity linear minimum mean square error (LMMSE) estimator for MIMO-OFDM HSR channels. The channel estimator utilizes a four-dimensional (4D) basis expansion channel model obtained from band-limited generalized discrete prolate spheroidal (GDPS) sequences. Exploiting the channel's band-limitation property, the proposed channel estimator outperforms the conventional interpolation based least square (LS) and MMSE estimators in terms of estimation accuracy and computational complexity, respectively. Simulation results demonstrate the robust performance of the proposed estimator for different delay, Doppler and angular spreads.

Channel state information (CSI) is required at the transmitter for improving the performance gain of the spatial multiplexing MIMO systems through linear precoding. In order to avoid the high data rate feedback lines, which are required in fast time-variant channels for updating the transmitter with the rapidly changing CSI, a subframe-wise channel tracking scheme is presented. The proposed channel predictor is based on an assumed DPS basis expansion model (DPS-BEM) for exploiting the variation of the channel coefficients inside each sub-frame and an auto regressive (AR) model of the basis coefficients over each transmitted frame. The proposed predictor properly exploits the channel's restriction to low dimensional subspaces for reducing the prediction error and the computational complexity. Simulation results demonstrate that the proposed channel predictor out-performs the DPS based minimum energy (ME) predictor for different ranges of normalized Doppler frequencies and has better performance than the conventional Wiener predictor for slower time-variant channels and almost the similar performance to it for very fast time-variant channels with reduced amount of computational complexity.

The work on the hybrid mm-wave channel estimator considers the sparse nature of the mm-wave channel in angular domain and leverages the compressed sensing (CS) tools for recovering the angular support of the MIMO-OFDM mm-wave channel.

The angular channel is treated in a continuous framework which resolves the limited angular resolution of the discrete sparse channel models used in the previous CS based channel estimators. The power leakage problem is also addressed by modelling the continuous angular channel as a multi-band signal with the bandwidth of each sub-band being proportional to the amount of power leakage. The RF combiner is designed to be implemented using a network of low-power switches for antenna subset selection based on a multi-coset sampling pattern. Simulation results validate the effectiveness of the proposed hybrid channel estimator both in terms of the estimation accuracy and the RF power consumption.

Contents

List of Tables

List of Figures

Abbreviations

AOA	Angle of Arrival
AOD	Angle of Departure
AR	Auto Regressive
BEM	Basis Expansion Model
BS	Base Station
CE	Complex Exponential
CS	Compressed Sensing
CSFT	Continuous Spatial Fourier Transform
CSI	Channel State Information
CSIT	Channel State Information at the Transmitter
DGMP	Distributed Grid Matching Pursuit
DPS	Discrete Prolate Spheroidal
DSFT	Discrete Spatial Fourier Transform
FDD	Frequency Division Duplex
GDPS	Generalized Discrete Prolate Spheroidal
HSR	High Speed Railway
LMMSE	Linear Minimum Mean Square Error
LMS	Least Mean Squares
LNA	Low Noise Amplifier
LOS	Line-of-Sight
LS	least square

LTE	Long Term Evolution
LTE-A	Long Term Evolution-Advanced
LTE-R	Long Term Evolution for Railway
ME	Minimum Energy
MIMO	Multiple-Input Multiple-Output
MMSE	Minimum Mean Square Error
MMV	Multiple Measurement Vectors
NLOS	Non-Line-of-Sight
NMSE	Normalized Mean Square Error
OFDM	Orthogonal Frequency Division Multiplexing
PCSI	Perfect Channel State Information
PM	Parametric Model
PRC	Parametric Radio Channel
RF	Radio Frequency
RFC	RF Chain
RLS	Recursive Least Squares
RS-GBSM	Regular Shape Geometry-Based Stochastic Model
RW-RLS	Rectangular-Windowed Recursive Least Squares
SISO	Single-Input Single-Output
SNR	Signal to Noise Ratio
SVD	Singular Value Decomposition
V2I	Vehicle to Infrastructure
V2V	Vehicle to Vehicle
WSSUS	Wide Sense Stationary Uncorrelated Scattering

Notations

Unless stated otherwise, lower case letters indicates scalers and boldface upper-case and lower-case letters denote matrices and vectors respectively.

a^*	the complex conjugate of the scaler a
$[\mathbf{a}]_i$	the ith element of vector $\mathbf{a}$
$[\mathbf{A}]_{i,j}$	the (i,j)th element of matrix $\mathbf{A}$
$\mathbf{A}[i,:]$	the ith row of matrix $\mathbf{A}$
$\mathbf{A}^{-1}$	the inverse of matrix $\mathbf{A}$
$\mathbf{A}^T$	the transpose of matrix $\mathbf{A}$
$\mathbf{A}^H$	the Hermitian transpose of matrix $\mathbf{A}$
$det(\mathbf{A})$	the determinant of matrix $\mathbf{A}$
$\mathbf{I}_n$	the $n \times n$ identity matrix
$\mathbb{R}$	the set of real numbers
$\mathbb{C}$	the set of complex numbers
$\mathbb{Z}$	the set of integers
$\mathbb{I}_n$	the set of non-negative integers $\{0, 1, \cdots, n-1\}$
$\lfloor a \rfloor$	the largest integer that is lower than or equal to a
$\lceil a \rceil$	The smallest integer that is greater than or equal to a
$\mathbf{a} \otimes \mathbf{b}$	The Kronecker product of $\mathbf{a}$ and $\mathbf{b}$

ACKNOWLEDGEMENTS

First and foremost, I like to express my greatest gratitude to my supervisor Dr. Xiaodai Dong. Her invaluable support, encouragement, guidance and comments paved the way through my PhD study and research.

I would also like to thank my supervisory committee members and external examiner Dr. Michael L. McGuire, Dr. Kui Wu, and Dr. Rose Qingyang Hu for offering me valuable comments and suggestions.

I would like to thank all my friends and colleagues at UVic for their help and support. Special thanks to my officemate Ali Jooya for his real friendship and support.

I would also like to thank my parents, my brother and my sister who are always supporting me and encouraging me through my whole life. I express my endless gratitude to my husband, Arash, for his unconditional support, help and love. Last but not least, I thank my lovely son, Kian, for being the greatest inspiration in my life.

Farnoosh Talaei, Victoria, BC, Canada

DEDICATION

To my parents, my husband, and my little son, Kian, for their endless support and love.

Chapter 1

Introduction

1.1 Research Areas Overview

With the fast development of high speed railways (HSRs), wireless communication for high speed trains has attracted more attentions in recent years. A main challenge of wireless communication for HSR is the rapidly time-varying and non-stationary propagation channel which together with the presence of line-of-sight (LOS) component and limited number of scatterers in most of the HSR scenarios, lead to violation of wide sense stationary uncorrelated scattering (WSSUS) condition [4]. The large Doppler and delay spread of the time-variant frequency-selective HSR channels, impose the high pilot overhead requirement for robust pilot-aided channel estimation. In order to reduce the required pilot overhead, a number of existing papers consider the restriction of doubly-selective channels to low-dimensional subspaces due to the channel's time and/or frequency correlation for single-input single-output (SISO) channel estimation. The direct application of reduced rank SISO channel estimation techniques for estimating the fast time-variant multiple-input multiple-output (MIMO) HSR channels can increase the required pilot overhead by several times based on the antenna arrays size. So, the first part of this dissertation is focused on MIMO orthogonal frequency-division multiplexing (OFDM) HSR channel estimation and a reduced rank channel estimator is proposed through representing the channel by a

4-dimensional (4D) basis expansion model (BEM) for further reducing the required pilot overhead.

Using multi-element antenna arrays at both the transmitter and the receiver sides has turned into an indispensable element of most wireless communication standards by offering higher capacity and performance gains compared to the SISO communication systems. Spatial multiplexing is a processing technique which improves the spectral efficiency of MIMO systems through sending multiple data streams over multiple transmit antennas simultaneously. Linear precoding can be used based on the available channel state information (CSI) at the transmitter side for adapting the data streams to the propagation channel and improving the performance gain of the spatial multiplexing MIMO systems. However, for the rapidly changing channel the CSI becomes out of date quickly and high data rate feedback lines are required for sending the estimated CSI to the transmitter for updating the precoder matrix. Channel prediction is a promising approach that can be used at the transmitter side to avoid high data rate feedback lines. So, as the second part of our work a reduced rank auto regressive (AR) channel predictor for fast time-variant narrowband MIMO channels is presented by exploiting the channel's restriction to low dimensional subspaces.

The mm-wave massive MIMO is a promising technology that enables Giga-bit-per second data rate communication through offering large bandwidth channels at mm-wave frequencies and the possibility of equipping the base stations with hundreds of small size antennas. There are several hardware constraints at mm-wave frequencies such as the high power consumption of the low noise amplifiers and the analog to digital/digital to analog converters at mm-wave frequencies and the space limitation for using a complete RF chain per each antenna which is the result of very close placement of antenna elements to each other. So, unlike lower frequencies where the signal processing is accomplished fully in the digital domain, for the mm-wave frequencies the fully baseband signal processing is a difficult task due to the high fabrication cost and power consumption of the RF circuits. Therefore, hybrid architectures are used for the efficient implementation of the precoding/combining process in a mixture of

analog and digital domains. The channel estimation is a challenging task for the hybrid architectures since the receiver experiences the channel through the analog precoding and/or combining circuits which intertwine the channel coefficients with the analog precoding and/or combining vectors and make it impossible to directly access the channel coefficients in the baseband domain. So, as the last part of this dissertation, a low-power hybrid channel estimation scheme is proposed for mm-wave MIMO-OFDM systems based on the sparse nature of the mm-wave channels in the angular domain and using the compressed sensing tools.

1.1.1 MIMO-OFDM HSR Channel Estimation

Conventional interpolation based channel estimators and parametric model channel estimation schemes require high pilot overhead for reliable channel estimation in rapidly-changing frequency-selective channels. Considering the fact that the time-variant frequency-selective channels are restricted to low dimensional subspaces, the basis expansion models have been proposed for reducing the channel estimation dimensions and consequently the required pilot overhead. For SISO-OFDM channel estimation, the BEM schemes exploit the channel's correlation in time and frequency domain and represent the time-varying channel's frequency response as a superposition of a few number of orthogonal basis. The channel estimation problem is thus converted to the estimation of the limited number of unknown basis coefficients. As for the fast time-varying MIMO-OFDM systems, one straightforward approach is to send training symbols from only one transmit antenna during a given time interval while keeping the other transmit antennas silent so that the channel frequency response of different antenna pairs can be obtained one by one using the same BEM schemes as the SISO-OFDM systems. The main drawback of this approach is the increase of the required pilot overhead which is proportional to the number of transmit antennas. To further reduce the pilot-overhead one can exploit the inherent spatial correlation between the multi-antenna elements which is imposed by the limited number of scatterers in most HSR scenarios. This motivates us to propose a reduced

rank channel estimator by modelling the channel based on the 4D generalized discrete prolate spheroidal (GDPS) sequences which exploit the time, frequency and spatial correlation of the MIMO-OFDM HSR channel, simultaneously. The proposed linear minimum mean square error (LMMSE) estimator outperforms the conventional least square (LS) estimator in terms of the estimation accuracy for the same pilot overhead. The proposed estimator overcomes the conventional MMSE estimator's requirement for the knowledge of the channel's second order statistics through approximating the time variant eigen-vectors of the channel's covariance matrix by time restricted and band limited GDPS sequences and has lower computational complexity compared to the MMSE estimator. The proposed reduced rank channel estimator is investigated in Chapter 2.

1.1.2 Time-variant MIMO Channel Prediction

Among different channel tracking schemes, BEM is the commonly used approach for expressing the time varying channel taps as superposition of some low dimensional time-varying basis functions such as complex exponential (CE) functions, polynomials and DPS sequences. So far the BEM channel prediction schemes are mainly focused on CE-BEM and polynomial-BEM channel prediction. However, it has been shown that the DPS-BEM outperform the CE-BEM and polynomial-BEM for approximating the Jacke's channel model. The time restriction and band limitation of the DPS basis motivates us to propose a sub-frame wise channel tracking scheme which considers the low dimensional DPS basis for modelling the channel's time-variation inside each sub-frame and applies an AR model approach for tracking the basis coefficients over each frame. The optimal subframe length and basis dimension are derived for a wide range of Doppler frequencies. The new channel predictor can be used for reduced feedback load and reduced feedback delay precoder design in time-variant MIMO channels. The proposed channel prediction scheme improves the prediction accuracy compared to the conventional AR predictor with lower computational complexity. It also has better performance than the DPS based minimum energy (ME) predictor over

different ranges of normalized Doppler frequencies. The proposed channel prediction scheme is presented in Chapter 3.

1.1.3 Hybrid MIMO-OFDM mm-Wave Channel Estimation

There are several publications which deal with the mm-wave channel estimation within the compressed sensing (CS) framework based on the sparse nature of the mm-wave channel in the angular domain. The previous CS-based mm-wave channel estimators can be divided into two groups, namely, the virtual and extended-virtual channel model approaches. The virtual channel model schemes apply the CS technique for estimation of the sparse discrete spatial Fourier transform of the mm-wave channel and the extended channel models leverage CS tools for recovering the limited number of quantized angles of arrival (AOAs) and angles of departure (AODs). The assumed discrete angular spectrum in the virtual channel model and the quantized angle grids of the extended virtual channel model restrict the accuracy the estimated channel. Moreover, the limited length of the antenna array results in the power leakage problem which reduces the sparsity level of the angular channel. To overcome the discretization/quantization problem of the previous discrete CS-based channel estimation schemes, a mm-wave channel estimation approach is proposed which treats the angular channel in a continuous framework and addresses the power leakage problem by exploiting the multi-band structure of the angular spectrum. The multiple measurement vectors (MMV) CS techniques are used for channel recovering through exploiting the same sparsity structure of the angular channel at all sub-carriers. A low power switch-based hybrid architecture is presented for implementing the proposed channel estimator which reduces the required number of RF chains. The proposed hybrid channel estimator outperforms the previous random CS based hybrid channel estimators in terms of the estimation accuracy, RF power consumption and base-band computational complexity. The corresponding analytical and simulation results are presented in Chapter 4.

1.1.4 Dissertation Organization

In Chapter 2, a reduced rank channel estimator for MIMO-OFDM HSR systems is proposed. Chapter 3 proposes a DPS based AR channel prediction approach for single carrier MIMO systems which can be used for precoder design in fast time-varying systems. Chapter 4 presents a hybrid channel estimation scheme for the mm-wave MIMO-OFDM systems. Finally, the research contributions on each topic are concluded in Chapter 5.

Chapter 2

Reduced Rank MIMO-OFDM Channel Estimation for High Speed Railway Communication using 4D Generalized DPS Sequences

2.1 Introduction

Wireless communication for HSRs has many important applications, including train safety, broadband communication services for passengers such as internet access and high quality voice or mobile video broadcasting [4]. In order to meet the broadband communication requirements for high speed trains, Long Term Evolution for Railway (LTE-R) based on LTE-Advanced (LTE-A) has been proposed [5, 6]. A main challenge of HSR wireless communication is the rapidly changing radio propagation condition. Thus, proper channel modelling and robust channel estimation and equalization are required for reliable wireless communication.

For HSR channel modelling several measurements campaigns have been conducted to measure the large-scale fading parameters, such as path loss and delay spread, in

different propagation environments such as cuttings, viaducts, crossing bridges and train stations [7, 8, 9, 10]. Moreover, a regular shape geometry-based stochastic model (RS-GBSM) for wideband multiple input multiple output (MIMO) HSR channels has been proposed in [1] which considers the time-variant small-scale fading parameters, such as AODs and AOAs for modelling the non-stationarity of the HSR scenarios.

Considering the large Doppler and delay spread of the time-variant frequency-selective HSR channel, the robust pilot aided channel estimation is a challenging task. For example, the LTE-A pilot pattern can not support high moving speeds [4]. Pilot aided OFDM channel estimation approaches can be divided into three groups, namely, interpolation based schemes, parametric model (PM) approaches and basis expansion models. The conventional interpolation based schemes use multi-dimensional interpolation of the estimated channel frequency response at pilots for reconstructing the channel at data locations. Papers [11] and [12] use 2D and 3D interpolation for SISO-OFDM and MIMO-OFDM channel estimation, respectively. The PM channel estimation schemes, use pilot symbols for directly estimating the multipath channel parameters such as the number of paths, path gains and delays, AOAs and AODs. The PM channel estimators have improved performance compared to the interpolation based schemes for the sparse multipath channels which can be modelled using a few number of parameters [13].

However, for rapidly time variant frequency selective channels both the interpolation based and PM schemes require high pilot overhead for tracking the time variation of the channel coefficients or multipath parameters inside each OFDM block. Considering the fact that doubly-selective channels are restricted to low-dimensional subspaces, several publications propose to use basis expansion models for further reducing the channel dimensions and consequently the required pilot overhead specifically for fast time-variant channels. Reference [14] propose a reduced rank channel estimator for each sub-carrier using the discrete prolate spheroidal (DPS) sequences. While [14] uses the time domain correlation for each sub-carrier, [15] and [16] propose low-dimensional channel estimators based on the frequency domain correlation

between sub-carriers via singular value decomposition (SVD) of the channel covariance matrix. Reference [15] assumes a known channel correlation matrix and [16] uses an adaptive manner to approximate the SVD of the correlation matrix. Further improvement can be obtained through exploiting time and frequency correlation simultaneously. Papers [17] and [18] use the time and frequency correlation and adopt the multi-dimensional DPS sequences in [14] to remove the requirement of the known covariance matrix. In [17] successive Slepian subspace projection of the channel is used in time and frequency and in [18] the eigen-vectors of the channel covariance matrix are approximated by a two-dimensional subspace model spanned by generalized-DPS (GDPS) sequences. In both papers, the channel estimation on different antennas are obtained one by one considering each antenna pair as a SISO-OFDM channel.

The 2D time-frequency DPS/GDPS sequences can be generalized to higher dimensions for exploiting the additional spatial correlation between the multi-antenna elements which is a common feature of most HSR scenarios that have a LOS component and limited number of scatterers due to the base station (BS) antenna heights and the distance of the BSs from the railway [4]. In [19], the projection of the known MIMO-OFDM channel coefficients onto 4D DPS sequences is used for low complexity implementation of a geometry-based channel model on a hardware channel simulator. For MIMO-OFDM channel estimation, However, to our best knowledge, none of the previous work has considered the extra spatial domain correlation together with the time and frequency correlation for obtaining a more accurate channel estimation with a lower pilot overhead. In this chapter we will use the spatial correlation to obtain a lower-dimensional channel model and achieve better performance with lower pilot overhead

Contributions:

1. A reduced rank linear minimum mean square error (LMMSE) channel estimator is proposed based on a 4D basis expansion channel model which uses GDPS sequences for exploiting the time, frequency and spatial correlation at the transmitter and receiver antenna arrays of a time-variant frequency-selective

MIMO-OFDM HSR channel.

2. The proposed time-variant channel estimator is validated using a RS-GBSM propagation channel.

2.2 System Model

We consider a MIMO-OFDM system shown in Fig.2.1. Each OFDM symbol contains N sub-carriers, and M_{T_x}-spatial data streams are equipped with M_{T_x} and M_{R_x} transmit and receive antennas, respectively. The transmission at each transmit antenna is frame based with frame length of M OFDM symbols. The system bandwidth is B and the OFDM symbol duration is given by $T_s = (N + G)T_c$ with G being the cyclic prefix length and $T_c = 1/B$. The transmitted symbol at the mth OFDM symbol, qth sub-carrier and sth transmit antenna is denoted by $d[m, q, s]$ and defined as:

$$d[m,q,s] = \begin{cases} b[m,q,s] & \text{if} \quad [m,q,s] \in \mathcal{S}_d \\ p[m,q,s] & \text{if} \quad [m,q,s] \in \mathcal{S}_p \\ 0 & \text{if} \quad [m,q,s] \notin \{\mathcal{S}_d \cup \mathcal{S}_p\} \end{cases} \tag{2.1}$$

where $b[m, q, s]$ and $p[m, q, s]$ is a QPSK modulated data symbol and pilot symbol, respectively. $\mathcal{S}_d \in \mathbb{Z}^3$ indicates the set of integer data locations and $\mathcal{S}_p \in \mathbb{Z}^3$ indicates the set of integer pilot locations. The received signal $y[m, q, r]$ over the rth receive antenna is the superposition of M_{T_x} data symbols sent from M_{T_x} transmit antennas at time m and sub-carrier q. That is,

$$y[m,q,r] = \sum_{s=1}^{M_{T_x}} h[m,q,r,s]d[m,q,s] + z[m,q,r] \tag{2.2}$$

where $h[m, q, r, s]$ is the sampled time-variant frequency response between the rth receive antenna and sth transmit antenna and $z[m, q, r]$ is the complex white Gaussian noise component. Section 2.3 provides more details of the channel model.

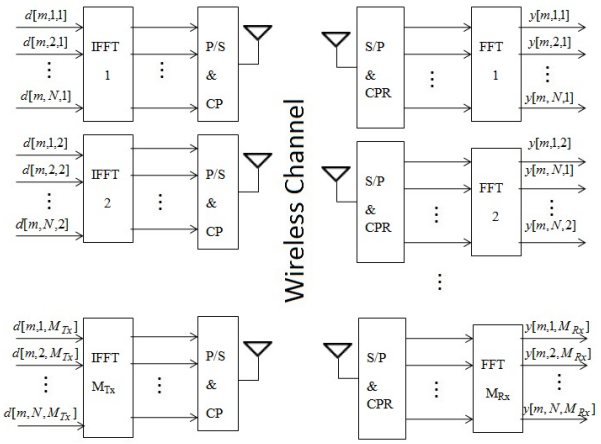

Figure 2.1: MIMO-OFDM system at time m

2.3 Geometry Based Stochastic Model for Wideband MIMO HST channel

For modelling the channel, we use the multi-tap RS-GBSM which is proposed recently for non-stationary wideband MIMO channels in high mobility railway communication [1]. As shown in Fig. 2.2 in this model the scatterers are assumed to be distributed over N_T confocal ellipses (N_T taps) with the BS and the receiver antenna arrays located at the foci. There are N_i effective scatterers on the ith ellipse. More details of the channel parameters are provided in Table 2.1 [1].

The time varying AODs and AOAs, for the scatterers located on the ith ellipse, are chosen from the von Mises distribution defined as follows for $\varphi_R^i(t)$ [1],

$$f(\phi_R^i)(t) = \exp[k_R^i \cos(\phi_R^i - \mu_R^i(t))]/[2\pi I_0(k_R^i)] \tag{2.3}$$

where μ_R^i is the mean angular value of AOA ϕ_R^i and k_R^i is the relevant von Mises parameter that controls the spread of ϕ_R^i. The relationship between the AOD and

Table 2.1: Parameter definitions of channel model [1]

$a_i(t)$,$b_i(t)$	Time varying semi-major and semi-minor axis of the ith ellipse
$D_s(t)$	Distance between the BS and the train
$f_s(t)$	$D_s(t)/2$
β_T, β_R,	Tilt angles of transmit and receive antenna array relative to x-axis, respectively
v_R,γ_R	Train velocity and angle of motion
Δ_x,Δ_y	Transmit and receive antenna element spacing
S_i	An scatterer located on the ith ellipse (the total number of scatteres on ith ellipse is N_i)
$\phi_T^i(t)$,$\phi_R^i(t)$	AOD and AOA corresponding to the scatterer S_i
$\phi_{los}^s(t)$	AOA of LOS component corresponding to sth transmit antenna
$E_T^i(t)$	Distance from the center of T_x array to the scatterer S_i
$E_R^i(t)$	Distance from the scatterer S_i to the center of the R_x array

AOA for multiple confocal ellipses model is given by [20]

$$\sin(\phi_T^i(t)) = \frac{b_i^2(t)\sin(\phi_R^i(t))}{a_i^2(t) + f_s^2(t) + 2a_i(t)f_s(t)\cos(\phi_R^i(t))} \tag{2.4}$$

$$\cos(\phi_T^i(t)) = \frac{2a_i(t)f_s(t) + (a_i^2(t) + f_s^2(t))\cos(\phi_R^i(t))}{a_i^2(t) + f_s^2(t) + 2a_i(t)f_s(t)\cos(\phi_R^i(t))} \tag{2.5}$$

where $a_i(t)$, $b_i(t)$ and $f_s(t)$ are defined in Table 2.1.

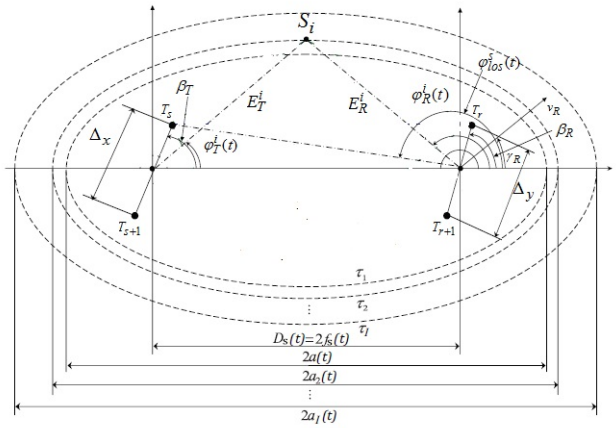

Figure 2.2: The GBSM for a wideband MIMO HST channel [1].

The channel is composed of the line-of-sight (LOS) component and non-LOS (NLOS) part, that is, the contribution from the diffuse scatterers in the environment. We can describe the channel by the time-variant transfer function $h(t, f, y, x) = h_{NLOS}(t, f, y, x) + h_{LOS}(t, f, y, x)$ with t, f, y and x denoting the time, frequency, po-

sition of the receive antenna on the receive antenna array and position of transmit antenna on the transmit antenna array, respectively. The NLOS channel is the superposition of the contribution from $P = \sum_{i=1}^{N_T} N_i$ multi-path components corresponding to total scatterers on all ellipses in Fig. 2.2, i.e.,

$$h_{NLOS}(t,f,y,x) = \sum_{i=1}^{P} \eta_i(t) e^{-j2\pi D_0/\lambda} e^{-j2\pi\tau_i(t)f} e^{j2\pi f_D \cos(\phi_R^i(t)-\gamma_R)t} \times e^{j2\pi y \cos(\phi_R^i(t)-\beta_R)/\lambda} e^{j2\pi x \cos(\phi_T^i(t)-\beta_T)/\lambda} \tag{2.6}$$

where $\eta_i(t)$ is the time variant amplitude of the ith path. The first exponential is the phase shift corresponding to the initial distance D_0 between the transmitter and receiver antenna arrays. f_D is the maximum Doppler frequency and the forth and fifth exponentials are phase shifts corresponding to the receive and transmit antenna position in the receive and transmit antenna arrays, respectively. $\tau_i(t) = \left(E_T^i(t) + E_R^i(t)\right)/c$ is the travel time of waves corresponding to the ith scatterer, c is the speed of light, and distances $E_T^i(t)$ and $E_R^i(t)$ defined in Table 2.1 can be obtained as [1]

$$E_T^i(t) = \frac{a_i^2(t) + f_s^2(t) + 2a_i(t)f_s(t)\cos(\phi_R^i(t))}{a_i(t) + f_s(t)\cos(\phi_R^i(t))} \tag{2.7}$$

$$E_R^i(t) = \frac{b_i^2(t)}{a_i(t) + f_s(t)\cos(\phi_R^i(t))} \tag{2.8}$$

Let $\Delta_f = 1/(NT_c)$ denote the width of a frequency bin and Δ_x and Δ_y denote the distance between adjacent antennas in the transmit and receive antenna arrays, respectively. The sampled NLOS channel transfer function can be described as a four

dimensional sequence

$$\begin{aligned} h_{NLOS}(m,q,r,s) &= h_{NLOS}(mT_s, \varphi(q)\Delta_f, k_r(r)\Delta_y, k_s(s)\Delta_x) \\ &= \sum_{i=1}^{P} \eta_i(m) e^{-j2\pi D_0/\lambda} e^{-j2\pi\tau_i(m)\varphi(q)\Delta_f} e^{j2\pi\upsilon_{max} m\cos(\phi_R^i(m)-\gamma_R)} \\ &\quad \times e^{j2\pi k_r(r)\Delta_y\cos(\phi_R^i(m)-\beta_R)/\lambda} e^{j2\pi k_s(s)\Delta_x\cos(\phi_T^i(m)-\beta_T)/\lambda} \end{aligned} \tag{2.9}$$

where $\upsilon_{max} = f_D T_s$ is the maximum normalized Doppler frequency and [18]

$$\varphi(q) = (q + \frac{N}{2})\mathrm{mod}(N) - \frac{N}{2} \tag{2.10}$$

maps the carrier index $q \in \{0, ..., N-1\}$ into the discrete frequency index $\varphi \in \mathrm{I}_Q = \{0, ..., N/2-1, -N/2, ..., -1\}$. Moreover [1],

$$k_s(s) = \frac{M_{T_x} - 2s + 1}{2} \tag{2.11}$$

$$k_r(r) = \frac{M_{R_x} - 2r + 1}{2} \tag{2.12}$$

map the transmit antenna index $s \in \{1, ..., M_{T_x}\}$ and receive antenna index $r \in \{1, ..., M_{R_x}\}$ into the discrete transmit antenna position index $k_s \in \mathrm{I}_S = \{(M_{T_x} - 1)/2, ..., -(M_{T_x}-1)/2\}$ and discrete receive antenna position index $k_r \in \mathrm{I}_R = \{(M_{R_x} - 1)/2, ..., -(M_{R_x}-1)/2\}$, respectively. Similarly for the LOS channel we can define

$$\begin{aligned} h_{LOS}(m,q,r,s) &= \eta_{los}(m) e^{j\phi} e^{-j2\pi D_0/\lambda} e^{-j2\pi\tau_{los}(m)\varphi(q)\Delta_f} e^{j2\pi\upsilon_{max} m\cos(\phi_{los}^s(m)-\gamma_R)} \\ &\quad \times e^{j2\pi k_r(r)\Delta_y\cos(\phi_{los}^s(m)-\beta_R)/\lambda} e^{j2\pi k_s(s)\Delta_x\cos(\beta_T)/\lambda} \end{aligned} \tag{2.13}$$

where η_{los} is the real amplitude of LOS component and can be estimated using the Rician K factor of the channel and the power of the first tap of h_{NLOS}. $\phi \in [-\pi, \pi)$, $\tau_{los}(t) = D_s(t)/c$ and $\phi_{los}^s(t)$ is the time-variant LOS AOA corresponding to the sth

transmit antenna shown in Fig. 2.2 and can be expressed as [21]

$$\phi_{los}^{s}(t) = \begin{cases} \phi_{los}^{s}(t_0) + \arccos\left(\frac{D_s(t_0)+v_R t\cos\gamma_R}{D_s(t)}\right), -\pi \leq \gamma_R \leq 0 \\ \phi_{los}^{s}(t_0) - \arccos\left(\frac{D_s(t_0)+v_R t\cos\gamma_R}{D_s(t)}\right), 0 \leq \gamma_R \leq \pi \end{cases} \tag{2.14}$$

where the initial LOS AOA is $\phi_{los}^{s}(t_0) = \arcsin\left(\frac{k_s \Delta_x}{D_s(t_0)}\sin(\beta_T)\right)$.

The amplitude η_i in (2.9) and the K factor of the channel depend on the scattering environments and are different in different propagation scenarios. More information will be provided in Section 2.6.

2.4 Generalized Discrete Prolate Spheroidal Channel Model

For channel estimation it is desirable to represent the MIMO-OFDM HST channel in time, frequency and spatial domain by a low dimensional subspace such that a low complexity reduced rank linear minimum mean square error (LMMSE) estimator can be employed. Generally, LMMSE estimator requires the knowledge of the second order statistics [22] which are either difficult or impossible to be estimated in rapidly changing HSR channels. In order to obtain a reduced-rank LMMSE, the eigenvectors of the covariance matrix are considered as the optimal basis for spanning a low dimensional subspace [15].

In this section we approximate the time-variant eigenvectors of the channel covariance matrix by a 4D subspace model spanned by GDPS sequences, which does not need the knowledge of the channel covariance matrix but only the ranges of the channel support in space, time and frequency domains. Section 2.4.1 provides an introduction to GDPS sequences and Section 2.4.2 explains the motivation for modelling the MIMO-OFDM HSR channel using a 4D subspace spanned by GDPS sequences.

2.4.1 DPS and GDPS Sequences

DPS sequences were first introduced by Slepian in 1987 [23] for approximation, prediction and estimation of band limited signals [24], [14]. The DPS sequences make a set of orthogonal basis that can span the same subspace U which is spanned by a time-concentrated and band-limited flat fading process with a symmetric spectral support $W = [-\nu_{max}, \nu_{max}]$. The DPS sequences $\{u_i[m, W, M]\}_{i=0}^{M-1}$ with band limitation to W and time concentration to $\mathbb{I}_M$ are the solutions to

$$\sum_{\ell=0}^{M-1} C[\ell - m, W] u_i[\ell, W, M] = \lambda_i(W, M) u_i[m, W, M] \tag{2.15}$$

where $m \in \mathbb{Z}$ and $C[k, W]$ is proportional to the covariance function of a process with constant spectrum over W and can be evaluated as [2],

$$C[k, W] = \int_W e^{j2\pi k\nu} d\nu \qquad \text{for } k \in \mathbb{Z} \tag{2.16}$$

and the eigenvalue $\lambda_i(W, M)$ represents the energy concentration of $u_i[m, W, M]$ within $\mathbb{I}_M$ and is given by

$$\lambda_i(W, M) = \frac{\sum_{m=0}^{M-1} |u_i[m, W, M]|^2}{\sum_{m=-\infty}^{\infty} |u_i[m, W, M]|^2}. \tag{2.17}$$

Later in [2], GDPS sequences were introduced by generalizing the concept of time-concentrated and band-limited sequences from a symmetric band-limiting interval to the union of I disjoint intervals which is shown in Fig. 2.3 and is expressed as following:

$$W = \bigcup_{i=1}^{I} B_i = B_1 \cup B_2 ... \cup B_I = [\upsilon_{11}, \upsilon_{12}] \cup [\upsilon_{21}, \upsilon_{22}] ... \cup [\upsilon_{I1}, \upsilon_{I2}] \tag{2.18}$$

The GDPS sequences are also obtained from (2.15), just by replacing the sym-

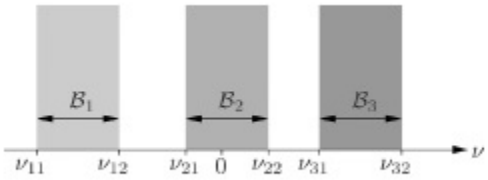

Figure 2.3: Band limiting region W consisting of I disjoint intervals [2]

metric W used for calculation of $C[k, W]$ by W defined in (2.18) which leads to

$$C[k, W] = \frac{1}{j2\pi k} \sum_{i=1}^{I} \left(e^{j2\pi k\nu_{i2}} - e^{j2\pi k\nu_{i1}} \right) \tag{2.19}$$

The essential dimension of the subspace U is given by [2]

$$D'(W, M) = \lceil |W|M \rceil + 1 \tag{2.20}$$

where for a highly oversampled fading process $|W| \ll 1$ and the process can be approximated by $D'(W, M) \ll M$ DPS/GDPS basis.

Motivated by the low dimensions of GDPS basis and considering the fact that the MIMO-OFDM HST channel is band limited in time, frequency and spatial domain, a 4D GDPS channel model for MIMO-OFDM HST channel will be presented in the next section.

2.4.2 4D GDPS Channel Model

In this section, based on the channel's band limitation in different domains, a 4D basis expansion model is used for the MIMO-OFDM HSR channel, which is similar to the 4D channel model presented in [19] but with the DPS basis being replaced by the GDPS sequences for having a more general model not necessarily being symmetric over its support in each domain. This model can be also used for wideband V2I or vehicle to vehicle (V2V) MIMO-OFDM channels. The band limitation of the channel

in time, frequency and space is defined based on the following properties,

1. The band limitation in time domain is controlled by the maximum normalized Doppler frequency of the channel which is defined as

$$\upsilon_{max} = \frac{\upsilon_R f_c}{c} T_s \tag{2.21}$$

where f_c is the carrier frequency. In fact the channel coefficients $h[m, q, r, s]$ for antenna pair $[r, s]$ and sub-carrier q over a finite time period $m \in \mathbb{I}_M$ is band-limited to maximum support $W_t = [-\upsilon_{max}, \upsilon_{max}]$. Note that within W_t there are at most P disjoint intervals corresponding to the Doppler spread of P scatterers. For the ith scatterer the Doppler spread is controlled by its time varying AOA, i.e., $\upsilon_D^i = \upsilon_{max} \cos(\phi_R^i(m) - \gamma_R)$.

2. For the frequency-domain subspace which models the channel coefficients $h[m, q, r, s]$ for the antenna pair $[r, s]$, a single OFDM symbol m and over all sub-carriers, i.e., $q \in \mathbb{I}_N$, the bandwidth is defined by the maximum normalized delay of the channel, θ_{max}, as given by

$$\theta_{max} = \frac{\tau_{max}}{N T_c} \tag{2.22}$$

Similarly within the maximum frequency support $W_f = [0, \theta_{max}]$, we can consider at most P disjoint intervals corresponding to P disjoint paths and each interval is controlled by time varying delay of the corresponding scatterer, i.e., $\theta_i = \tau_i(m)\Delta_f$.

3. The band-limitation in the spatial domain is based on non-isotropic scattering environments. Although in some HSR scenarios such as cuttings we can consider uniform distribution of scatterers at two sides of the track, not all of the power scattered by the scatterers will be received by the train [25]. Non-isotropic scattering is also confirmed by measurements of WINNER II project

[26]. Considering (2.9), the spatial domain band-limitation for the receiver can be described by the maximum and minimum normalized AOA defined as

$$\xi_{max} = \max\{\cos(\phi_R^i(m) - \beta_R)\}\frac{\Delta_y}{\lambda}$$
$$\xi_{min} = \min\{\cos(\phi_R^i(m) - \beta_R)\}\frac{\Delta_y}{\lambda} \tag{2.23}$$

where the maximization (minimization) is among all scatterers and over the whole observation time. The maximum support of the AOA $W_y = [\xi_{min}, \xi_{max}]$ can also have P disjoint intervals corresponding to P disjoint time-varying AOAs.

4. Similarly we can define the spatial band limitation at the transmitter using the normalized maximum and minimum AODs defined as,

$$\zeta_{max} = max\{\cos(\phi_T^i(m) - \beta_T)\}\frac{\Delta_x}{\lambda}$$
$$\zeta_{min} = min\{\cos(\phi_T^i(m) - \beta_T)\}\frac{\Delta_x}{\lambda} \tag{2.24}$$

The maximum support of the AOD is $W_x = [\zeta_{max}, \zeta_{max}]$ which can have at most P disjoint intervals corresponding to the P time-varying AODs.

In summary it can be seen that the maximum bandwidth of $h[m, q, r, s]$ is restricted to

$$W_{max} = W_t \times W_f \times W_x \times W_y. \tag{2.25}$$

The band-limitation property of a MIMO-OFDM HSR channel allows us to represent the channel of all antennas over a frame of M OFDM symbols by the following 4D

subspace model

$$h[m,q,r,s] = \sum_{d_t=0}^{D_t-1}\sum_{d_f=0}^{D_f-1}\sum_{d_y=0}^{D_y-1}\sum_{d_x=0}^{D_x-1} U_{d_t}^{t}[m,W_t,M]U_{d_f}^{f}\left[\varphi(q)+\frac{N}{2},W_f,N\right]$$
$$\cdot U_{d_y}^{y}\left[k_r(r)+\frac{M_{R_x}}{2},W_y,M_{R_x}\right]U_{d_x}^{x}\left[k_s(s)+\frac{M_{T_x}}{2},W_x,M_{T_x}\right]\psi_{d_t,d_f,d_y,d_x} \quad (2.26)$$

where the GDPS basis $\{U_{d_t}^{t}[m,W_t,M], m\in\mathbb{I}_M, d_t\in\mathbb{I}_{D_t}\}$, $\{U_{d_f}^{f}[q,W_f,N], q\in \mathrm{I}_Q, d_f\in \mathbb{I}_{D_f}\}$, $\{U_{d_y}^{y}[r,W_y,M_{R_x}], r\in \mathrm{I}_R, d_y\in\mathbb{I}_{D_y}\}$, $\{U_{d_x}^{x}[s,W_x,M_{T_x}], s\in \mathrm{I}_S, d_x\in\mathbb{I}_{D_x}\}$ span the time, frequency, receiver spatial domain and transmitter spatial domain subspaces respectively. ψ_{d_t,d_f,d_y,d_x} is the corresponding weighting coefficient for these basis. D_t, D_f, D_y, D_t are the essential dimensions of time, frequency and spatial domains subspaces, respectively, defined as

$$D_t = \lceil |W_t|M \rceil + 1$$
$$D_f = \lceil |W_f|N \rceil + 1$$
$$D_y = \lceil |W_y|M_{R_x} \rceil + 1$$
$$D_x = \lceil |W_x|M_{T_x} \rceil + 1. \quad (2.27)$$

For modern high-rate communication systems, maximum normalized Doppler frequency $\upsilon_{max} << 1$ which implies $|W_t| << 1$ and consequently $D_t << M$. Similarly, as the maximum excess delay is limited in communication systems, the maximum support of the normalized power delay profile is $|W_f| << 1$ and so $D_f << N$. Considering non-isotropic scattering with limited AOD and AOA spread and the proper distance between the antennas in transmit and receive antenna arrays, we also have $D_x << M_{T_x}$ and $D_y << M_{R_x}$.

2.5 Channel Estimation

In this section we will present an LMMSE channel estimator based on the 4D GDPS channel model of (2.26).

2.5.1 Problem Formulation

Considering the channel model obtained in (2.26), we can reformulate the signal model in (2.2) as

$$y[m,q,r] = \sum_{s=1}^{M_{T_x}} \sum_{d_t=0}^{D_t-1} \sum_{d_f=0}^{D_f-1} \sum_{d_y=0}^{D_y-1} \sum_{d_x=0}^{D_x-1} U_{d_t}^t[m] U_{d_f}^f \left[\varphi(q) + \frac{N}{2}\right] U_{d_y}^y \left[k_r(r) + \frac{M_{R_x}}{2}\right] \times U_{d_x}^x \left[k_s(s) + \frac{M_{T_x}}{2}\right] \psi_{d_t,d_f,d_y,d_x} d[m,q,s] + z[m,q,r] \tag{2.28}$$

where for notation simplicity, in (2.28) and in the rest of this chapter, we omit the index set and bandwidth notations used previously in the definition of GDPS basis. Using equation (2.28), the channel estimation problem is now reduced to estimation of the basis coefficients. The number of coefficients required to be estimated $|\psi_{d_t,d_f,d_y,d_x}| = D_t D_f D_y D_x << MNM_{R_x}M_{T_x}$. To obtain ψ_{d_t,d_f,d_y,d_x}, we can rewrite (2.28) in the matrix-vector form. We collect all basis coefficient in the vector Ψ with the following order,

$$\Psi[d_t D_f D_y D_x + d_f D_y D_x + d_y D_x + d_x + 1] = \psi_{d_t,d_f,d_y,d_x} \tag{2.29}$$

Similarly we define vectors $\mathbf{y}$ and $\mathbf{z}$ containing the the received data values $y[m,q,r]$ and corresponding noise values $z[m,q,r]$ from all antennas over the transmitted frame as

$$\begin{aligned} \mathbf{y}[mNM_{R_x} + qM_{R_x} + r + 1] &= y[m,q,r] \\ \mathbf{z}[mNM_{R_x} + qM_{R_x} + r + 1] &= z[m,q,r]. \end{aligned} \tag{2.30}$$

From (2.29) and (2.30) we can define the final input-output relationship as

$$\mathbf{y} = \mathbf{D}\Psi + \mathbf{z} \tag{2.31}$$

where $\mathbf{D}$ is an $MNM_{Rx} \times D_t D_f D_y D_x$ matrix whose rows are given by

$$\mathbf{D}\left[mNM_{R_x} + qM_{R_x} + r, :\right] = \underbrace{\mathbf{f}^t[m] \otimes \mathbf{f}^f[q] \otimes \mathbf{f}^y[r]}_{D_1[m,q,r]} \otimes \mathbf{f}^d[m,q] \tag{2.32}$$

with

$$\begin{aligned}
\mathbf{f}^t[m] &= \left[U_0^t[m], \ldots, U_{D_t-1}^t[m]\right] \\
\mathbf{f}^f[q] &= \left[U_0^f\left[\varphi(q) + \frac{N}{2}\right], \ldots, U_{D_f-1}^f\left[\varphi(q) + \frac{N}{2}\right]\right] \\
\mathbf{f}^y[r] &= \left[U_0^y\left[k_r(r) + \frac{M_{R_x}}{2}\right], \ldots, U_{D_y-1}^y\left[k_r(r) + \frac{M_{R_x}}{2}\right]\right] \\
\mathbf{f}^x[s] &= \left[U_0^x\left[k_s(s) + \frac{M_{T_x}}{2}\right], \ldots, U_{D_x-1}^x\left[k_s(s) + \frac{M_{T_x}}{2}\right]\right] \\
\mathbf{f}^d[m,q] &= \sum_{s=1}^{M_{T_x}} \mathbf{f}^x[s]\, d[m,q,s].
\end{aligned} \tag{2.33}$$

Note that in (2.32), D_1 only depends on the GDPS basis and $\mathbf{f}^d$ is the pilot (data) dependent part.

2.5.2 LMMSE Estimation of Basis Expansion Coefficients

The linear estimator for the basis coefficient vector in (2.31) is expressed as [27]

$$\hat{\Psi}_{LMMSE} = \mathbf{C}_{\mathbf{y}\Psi}^H \mathbf{C}_{\mathbf{yy}}^{-1} \mathbf{y} \tag{2.34}$$

and covariance matrices are given by

$$\mathbf{C}_{\mathbf{yy}} = \underset{d}{\mathbb{E}}\underset{\Psi}{\mathbb{E}}\underset{\mathbf{z}}{\mathbb{E}}\left\{\mathbf{y}\mathbf{y}^H\right\} = \underset{d}{\mathbb{E}}\left\{\mathbf{D}\mathbf{C}_\Psi\mathbf{D}^H\right\} + \sigma_z^2\mathbf{I}_{MNM_{R_x}} \tag{2.35}$$

$$\mathbf{C}_{\mathbf{y}\Psi} = \underset{d}{\mathbb{E}}\underset{\Psi}{\mathbb{E}}\underset{\mathbf{z}}{\mathbb{E}}\left\{\mathbf{y}\Psi^H\right\} = \underset{d}{\mathbb{E}}\left\{\mathbf{D}\mathbf{C}_\Psi\right\} = \tilde{\mathbf{D}}\mathbf{C}_\Psi \tag{2.36}$$

where σ_z^2 is the noise variance and $\tilde{\mathbf{D}}$ is obtained by replacing $d[m,q,s]$ in matrix $\mathbf{D}$ by $\tilde{d}[m,q,s]$ defined as

$$\tilde{d}[m,q,s] = \begin{cases} d[m,q,s] & \text{if} \quad [m,q,s]^T \in \mathcal{S}_p \\ 0 & \text{if} \quad [m,q,s]^T \notin \mathcal{S}_p \end{cases} \tag{2.37}$$

which means that only pilot symbols are used for channel estimation. For the presented 4D GDPS channel model the covariance matrix $\mathbf{C}_\Psi$ is given by

$$\mathbf{C}_\Psi = \frac{1}{|W_t|\,|W_f|\,|W_y|\,|W_x|} diag\left(\lambda_t \otimes \lambda_f \otimes \lambda_y \otimes \lambda_x\right) \tag{2.38}$$

with

$$\begin{aligned} \lambda_t &= \left[\lambda_0^t, ..., \lambda_{D_t-1}^t\right] \\ \lambda_f &= \left[\lambda_0^f, ..., \lambda_{D_f-1}^f\right] \\ \lambda_y &= \left[\lambda_0^y, ..., \lambda_{D_y-1}^y\right] \\ \lambda_x &= \left[\lambda_0^x, ..., \lambda_{D_x-1}^x\right] \end{aligned} \tag{2.39}$$

contain the eigenvalues defined by (2.17) for each of the GDPS basis.

Replacing the covariance matrices in (2.34), the LMMSE estimation of the basis coefficients is obtained as

$$\hat{\Psi}_{LMMSE} = \left(\tilde{\mathbf{D}}^H \Delta^{-1} \tilde{\mathbf{D}} + \mathbf{C}_\Psi^{-1}\right)^{-1} \tilde{\mathbf{D}}^H \Delta^{-1} \mathbf{y} \tag{2.40}$$

where

$$\Delta = \Lambda + \sigma_z^2 \mathbf{I}_{MNM_{R_x}}, \tag{2.41}$$

and the block-diagonal matrix Λ is expressed as

$$\Lambda\left[i_{m,q,r_1}, i_{m,q,r_2}\right] = \frac{1}{|W_t||W_f||W_y||W_x|} \sum_{d_t=0}^{D_t-1} \sum_{d_f=0}^{D_f-1} \sum_{d_y=0}^{D_y-1} \sum_{d_x=0}^{D_x-1}$$
$$\left\{ \lambda_{d_t}^t \lambda_{d_f}^f \lambda_{d_y}^y \lambda_{d_x}^x \left|U_{d_t}^t[m]\right|^2 U_{d_y}^y[k_r(r_1) + \frac{M_{R_x}}{2}] U_{d_y}^y[k_r(r_2) + \frac{M_{R_x}}{2}]^* \right.$$
$$\left. \left|U_{d_f}^f[\varphi(q) + \frac{N}{2}]\right|^2 \sum_{s=1}^{M_{T_x}} \left|U_{d_x}^x[k_s(s) + \frac{M_{T_x}}{2}]\right|^2 \left(1 - \left|\tilde{d}[m,q,s]\right|^2\right) \right\} \qquad (2.42)$$

with $i_{m,q,r_i} = mNM_{R_x} + qM_{R_x} + r_i$ for $i = 1, 2$ and $r_1, r_2 \in \{1, ..., M_{R_x}\}$.

2.6 Simulation Results

In this section, we present the simulation results to evaluate the proposed channel estimator. We consider $M = 14$, $N = 128$, $M_{T_x} = M_{R_x} = 4$, $f_c = 1.8$ GHz, $T_s = 8$ μs, $B = 1/T_c = 20$ MHz and the channel parameters listed in Table 2.2 or specified otherwise. The maximum normalized Doppler spread is controled by the train velocity v_R as $|W_t| = 2\upsilon_{max} = 2v_R f_c T_s/c$ and considering the adjacent channel taps are at distance T_c from eachother, the maximum normalized delay spread is $|W_f| = \theta_{max} = N_T/N$. According to (2.3) the time varying AODs and AOAs of different scatterers are chosen from the von Mises distribution controlling the angular spread and correspondingly the maximum support of the channel in spatial domain based on (2.23) and (2.24).

Table 2.2: Channel parameters for the RS-GBSM described in Section 2.3 [1]

D_0	D_{min}	γ_R	β_T	β_R	N_T	N_i	υ_R	Δ_x	Δ_y
100 m	30 m	22.5^o	22.5^o	22.5^o	10	50	$100(m/s)$	$\lambda/2$	$\lambda/2$

Viaducts and cuttings are the two most common HSR propagation environments which are special and different from those in commercial cellular communication [4]. The measurements in [28] show that the propagation environment of terrain cutting

is worse than viaduct. So we consider the cutting scenario, shown in Fig. 2.4, for our simulation.

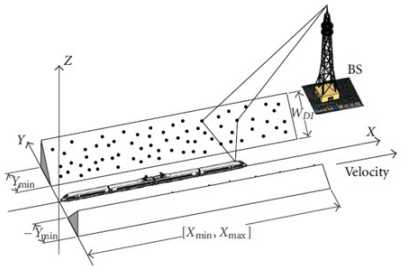

Figure 2.4: Cutting scenario [3]

The complex path amplitude of the scatterers diffused on the surface of two slopes of the train cutting is modelled as

$$\eta_i(t) = G_{0,DI}^{1/2}.c_i.\left(\frac{d_{ref}}{d_{T\to i}(t) \times d_{i\to R}(t)}\right)^{n_{DI}/2} \tag{2.43}$$

where c_i is the zero mean complex Gaussian gain of the ith scatterer. $n_{DI} = 3$, $G_{0,DI} = 23$ dB are the path loss exponent and reference power and $d_{T\to i}$ and $d_{i\to R}$ are the scatterer distance to the BS and to the train, respectively. The Ricean K factor in the cutting scenario follows the log-normal distribution with the mean 0.94 dB and standard deviation 4.18 dB [3].

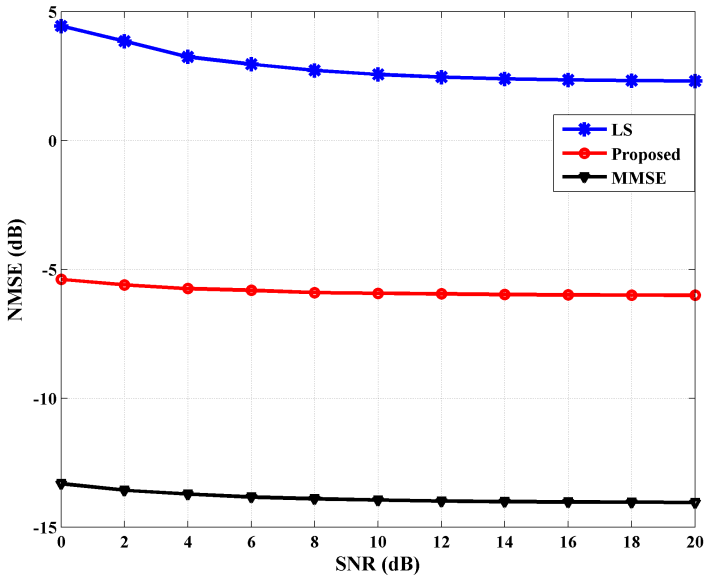

Figure 2.5: Comparison of different estimators with the pilot overhead of 0.0135 for a 4×4 MIMO-OFDM system with $|W_t| = 0.0096$, $|W_f| = 0.0781$, AOA spread of 35.2° and AOD spread of 43.5°.

Fig. 2.5 compares the performance of the proposed GDPS-based channel estimator in terms of the normalized mean square error (NMSE) with the conventional interpolation based LS and MMSE estimators which require to first obtain the channel estimation at pilot positions and then use a 2D interpolation in time and frequency to obtain the channel coefficients at the rest of the sub-carriers for each antenna pair. The 3D diamond pilot pattern presented in [12] is used for multiplexing the pilots into the transmitted data stream. The pilot overhead of diamond grid is adjustable based on the essential dimension of the GDPS basis in time, frequency and transmitter spatial domain which according to (2.27) are proportional to the bandwidth of the channel in each domain. The proposed channel estimator has better performance than the LS estimator. However, the MMSE channel estimator outperforms the proposed scheme since the MMSE approach uses the full channel correlation information for both channel estimation at the pilot sub-carriers and interpolation at the data sub-carriers.

Fig. 2.6 shows the performance of the proposed channel estimator for different AOD and AOA spreads. For all cases it is assumed that $D_t = 2$, $D_f = 11$ and

$D_x = 2$, leading to the same pilot overhead of 0.0135. Since the same number of basis are used for spanning the transmitter spatial domain, the performance degrades for bigger AOD spreads. Moreover, for bigger AOA spreads more GDPS basis may be used for channel modelling which improves the estimation accuracy. The average D_y is indicated for each case. The effect of different antenna sizes is investigated in Fig. 2.7 for the same pilot overhead. Increasing the number of antennas will increase the number of basis used for channel modelling and can provide better channel approximation. However, for the transmitter array the increased number of antennas degrades the performance since the pilot overhead in the transmitter spatial domain is the same for all antenna sizes. For the receiver spatial domain, as the channel is sampled at all receive antennas we have enough samples for estimating the increased number of basis coefficients. So better performance is obtained for the bigger receiver antenna array sizes.

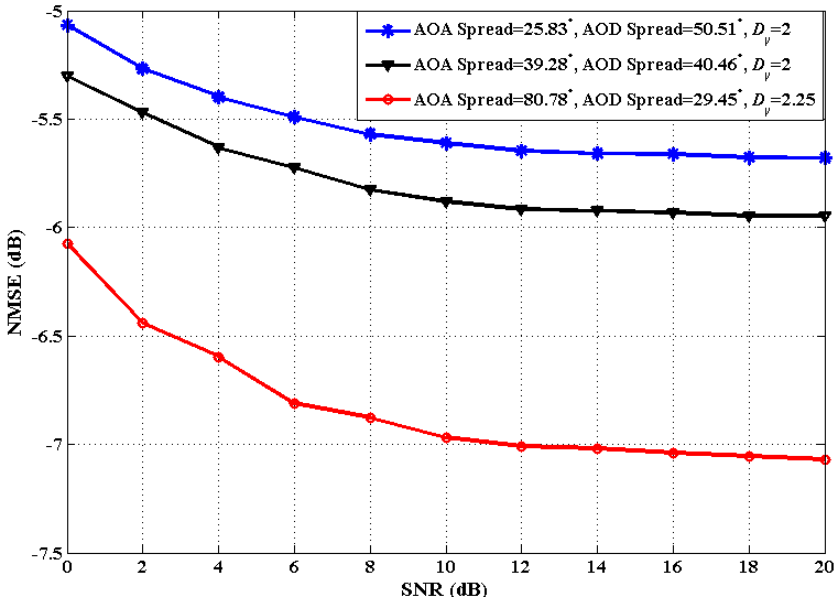

Figure 2.6: Evaluation of the proposed channel estimator for different AOD/AOA spreads for a 4×4 MIMO-OFDM system with the pilot overhead of 0.0135, $|W_t| = 0.0096$ and $|W_f| = 0.0781$.

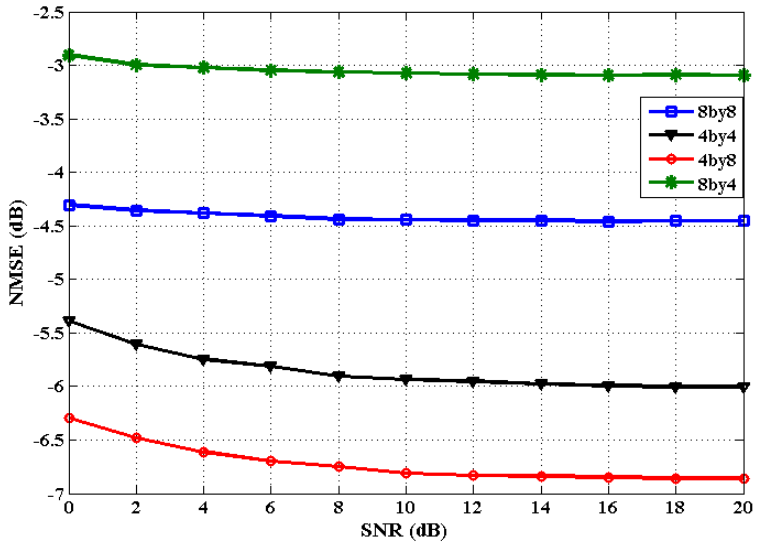

Figure 2.7: Evaluation of the proposed channel estimator for different number of antennas with the pilot overhead of 0.0135, AOA spread of 35.2°, AOD spread of 43.5°, $|W_t| = 0.0096$ and $|W_f| = 0.0781$.

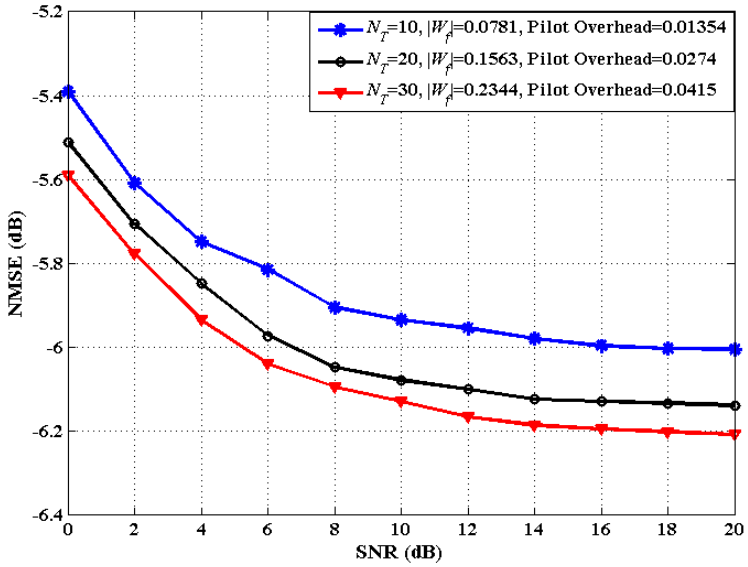

Figure 2.8: Evaluation of the proposed channel estimator for different delay spreads with the AOA spread of 35.2°, AOD spread of 43.5° and $|W_t| = 0.0096$.

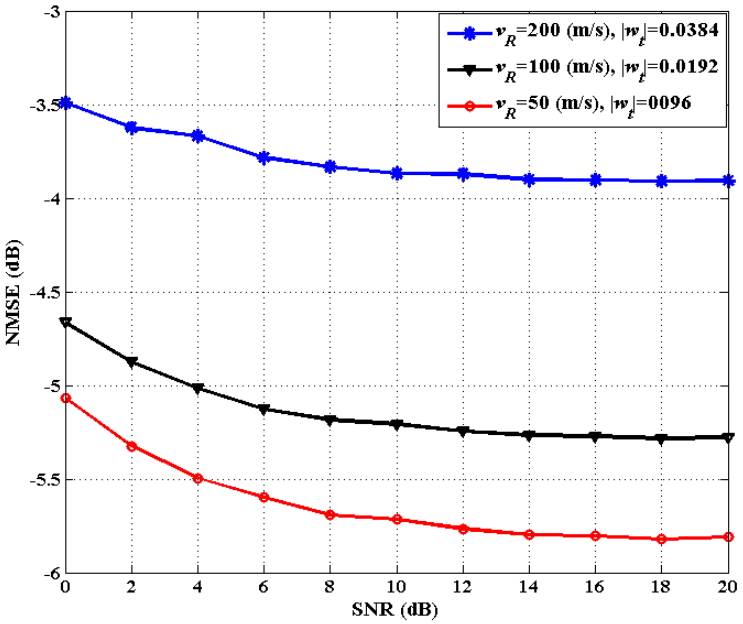

Figure 2.9: Evaluation of the proposed channel estimator for different train velocities with $M = 28$, $T_s = 16$ μs, $B = 10$ MHz, AOA spread of 35.2°, AOD spread of 43.5° and $|W_f| = 0.0781$.

Fig. 2.8 represents the effect of different delay spreads on channel estimation accuracy. Each scenario has a distinct pilot overhead based on the distinct number of frequency domain basis. As the pilot overhead is adjusted to each scenario it is expected that the NMSE does not differ greatly for each case. Fig. 2.9 also indicates the performance of the proposed channel estimator for different Doppler spreads. It is obvious that for the same pilot overhead, the bigger the train velocity is, the worse it is the channel estimator performance.

The computational complexity of the proposed reduced rank LMMSE estimator (2.40) in terms of floating point operations, is determined by the dimension of $\tilde{\mathbf{D}} \in \mathbb{C}^{MNM_{Rx} \times D_t D_f D_y D_x}$ and is calculated as follows [29]

$$C_{GDPS} \approx 8MNM_{Rx} \left(D_t D_f D_y D_x\right)^2 + \frac{8}{3} \left(D_t D_f D_y D_x\right)^3, \tag{2.44}$$

while for a full rank LMMSE estimator in which the channel coefficients are estimated rather than the basis coefficients, $\tilde{\mathbf{D}} \in \mathbb{C}^{MNM_{Rx} \times MNM_{Rx} M_{Tx}}$ and the computational

complexity is

$$C_{full} \approx 8\left(MNM_{Rx}\right)^3 \left({M_{Tx}}^2 + \frac{1}{3}{M_{Tx}}^3\right). \tag{2.45}$$

As an example, for the parameters presented in Table 2.2 with 8×8 MIMO size, $D_t = 2$, $D_f = 11$, $D_y = 3$ and $D_x = 3$, there is relative complexity reduction of $C_{full}/C_{GDPS} = 1.2246e + 06$.

2.7 Conclusion

Considering the time, frequency and spatial correlation of the MIMO-OFDM HSR channels, we have proposed a reduced rank LMMSE estimator based on a 4D GDPS channel model. The low dimension of the basis resulted in the good performance of the GDPS based channel estimator compared to the conventional interpolation based LS and MMSE channel estimators for the same pilot overhead and with lower computational complexity. Simulation results, presented for the train cutting scenario and the non-stationary RS-GBSM channel model, have demonstrated the robust performance of the channel estimator for different antenna sizes and different Doppler, delay and angular spreads.

Chapter 3

MIMO Channel Prediction for Fast Time-Variant Flat Fading Channels based on Discrete Prolate Spheroidal Sequences

3.1 Introduction

Multiple-input multiple-output (MIMO) wireless communication attracted high attention during the past decades due to its capability for providing higher capacity and performance gains compared to single-input single-output (SISO) systems. High spectral efficiency can be achieved in MIMO systems through sending multiple data streams simultaneously over multiple transmit antennas, which is called spatial multiplexing [30]. The performance of spatial multiplexing can be further improved if the transmitted streams are matched to the propagation channel. Linear precoding is a technique that uses the available channel state information (CSI) at the transmitter (CSIT) for adapting the data streams to the instantaneous propagation channel [31], [32]. In frequency division duplex (FDD) systems the CSIT can be obtained through

the feedback technique. However, the feedback load and feedback delay should be minimized for fast and reliable communication. The feedback load can be reduced by sending some quantized form of CSI through the feedback channel [33, 34, 35]. The feedback delay is also an important issue especially in fast time-variant channels which leads the CSIT to become out of date and degrades the performance of the precoder. Channel prediction has been proposed as a promising scheme to overcome the feedback delay problem [36, 37].

Channel prediction techniques can be mostly divided into three groups, the parametric radio channel (PRC) model, the auto regressive (AR) model and basis-expansion model (BEM) [38]. The PRC approach models the time-variant channel as a sum of complex sinusoids each of which is determined with its amplitude and Doppler frequency. The parameters associated with each complex sinusoid is estimated using the known channel coefficients and will be used for channel prediction. References [39, 40, 41, 42] used the PRC method for SISO channel prediction and [43], [44] applied PRC for MIMO and Multi-user MIMO channel prediction, respectively.

The conventional AR schemes use a linear minimum mean square error (MMSE) filter for predicting the future channel as a linear combination of the known channel coefficients [45, 46, 40, 47, 48]. This requires the knowledge of channel correlation matrix. For the case of unknown or time-variant correlation function, adaptive AR schemes have been developed which are based on adaptive filtering techniques such as least mean squares (LMS) [49], recursive least squares (RLS) [50] and Kalman filtering [37], [51]. For AR models the computational complexity grows with the number of antennas when they are extended for MIMO channel prediction [52].

BEM is a widely used type of channel representation for time varying systems where the time varying channel taps can be approximated as a linear combination of some low dimensional orthogonal basis such as complex exponential (CE) functions, polynomials, Discrete Prolate Spheroidal (DPS) Sequences, etc. The basis are determined based on the channel's Doppler spread and the basis coefficients are estimated using the channel information at pilot positions. Papers [53] and [54] consider

polynomial-BEM channel tracking in which basis coefficients are updated frame by frame using the rectangular-windowed RLS (RW-RLS) adaptive filtering and Kalman filtering schemes, respectively. Paper [53] also provides a method to obtain the polynomial optimal model order. Channel tracking using CE-BEM has been investigated in several papers [55, 56, 57]. Reference [55] uses a Kalman filtering scheme based on an assumed first-order Gauss-Markov model of CE-BEM coefficients for tracking the basis coefficients from one OFDM block to the next. In [56], the transmitted symbols are segmented into over-lapping blocks each containing several sub-blocks and differing from its adjacent blocks only by one sub-block. The sub-block wise updating of the CE-BEM coefficients for each block is performed using a Kalman filtering scheme for an assumed first-order AR model of basis coefficients and also using an RLS algorithm without considering any model for basis coefficients. A similar tracking scheme to [56] is also proposed in [57] where the extra information from the decision symbols is considered together with the information from the training sessions for improving the estimation of CE-BEM coefficients.

DPS-BEM is another commonly used BEM which is shown to outperform the polynomial-BEM and CE-BEM in approximating the Jacke's channel model for different ranges of Doppler spreads [58]. Several publications have considered the low dimensional channel estimation based on the DPS basis [59, **?**]. As for the channel tracking, [60] proposes a minimum energy (ME) extrapolation-based predictor where the time-concentrated and band-limited DPS sequences are used for approximating the channel over a period of time for which the channel coefficients are known (estimated). The same estimated basis coefficients together with the same extrapolated DPS basis are used for the prediction of the future channel samples. Although ME predictor has low complexity, its performance degrades for long range prediction over fast time-variant channels [38].

In this chapter we develop a new DPS-BEM channel predicting scheme which assumes non-overlapping transmitted frames and applies a sub-frame wise tracking approach for updating the DPS-basis coefficients based on a Q-order AR modelling of

the basis coefficients. The proposed scheme differs from the sub-block wise CE-BEM tracking approchs of [56, 57] in that they exploit the CE basis for the overall channel variation in each frame which implies the basis duration being the same as the frame duration and increases the required number of CE basis for channel modelling. Since the frame length is large, overlapping frames are considered for better tracking of the basis coefficients. However, for the proposed DPS-BEM tracking scheme a few number of DPS basis which are time-limited to the sub-frame length are used for exploiting the channel variation inside each sub-frame and an AR model is applied for tracking the channel variation between subframes without any requirement for considering overlapping frames. Moreover, the CE-BEM tracking schemes of [56, 57] consider time-multiplexed training sessions inside each subframe for updating the basis coefficients, while the proposed frame structure only assumes known channel coefficients at the beginning of each frame. The detailed contributions are as follows:

1. We formulate the channel prediction problem considering a DPS-BEM of the time-variant channel coefficients over each sub-frame and an AR model of the time-variant DPS basis coefficients over the whole transmitted frame. The error contribution from the AR prediction of the DPS basis coefficients and the DPS modelling of the channel coefficients is investigated and an algorithm for obtaining the optimal sub-frame length (correspondingly the optimal AR modelling order) and the optimal number of basis per sub-frame is proposed through minimizing the total prediction error of the transmitted frame.

2. The application of the proposed channel predictor for reduced feedback load and delay precoder design is investigated and the relative amount of feedback load reduction is obtained for different MIMO sizes. The performance of the proposed channel predictor is evaluated for the Jakes's fading channel model with different normalized Doppler spreads and the results are compared with the ME and the conventional AR predictors.

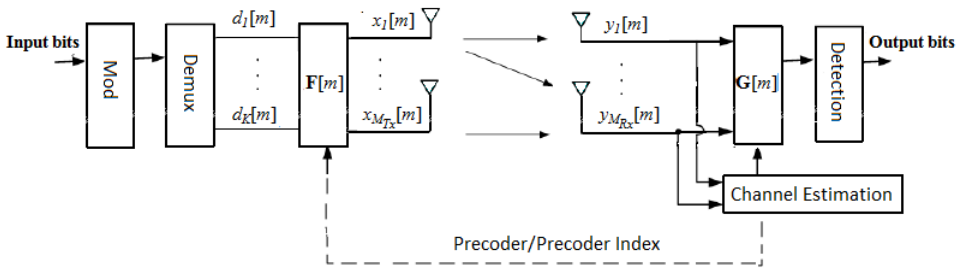

Figure 3.1: Precoded MIMO system at time m

3.2 System Model

A precoded MIMO system with M_{Tx} transmit antennas and M_{Rx} receive antennas is shown in Fig. 3.1. The input bit stream is first QPSK modulated and then it is demultiplexed into K-spatial data streams represented by $\{d_i[m]\}_{i=1}^{K}$ at time m. Note that $K \leq M_{Rx} \leq M_{Tx}$ in general and for a full-rate system $K = M_{Rx} = M_{Tx}$ which is assumed in the rest of this chapter without loss of generality. Considering $\mathbf{d}[m] = [d_1[m], d_2[m], \cdots, d_{M_{Tx}}[m]]^T$ as a vector which contains the mth symbol of all data streams, this vector is then multiplied by the precoder matrix $\mathbf{F}[m]$ to obtain the transmitted symbols as

$$\mathbf{x}[m] = \mathbf{F}[m]\mathbf{d}[m] \tag{3.1}$$

where $\mathbf{x}[m] = [x_1[m], x_2[m], \cdots, x_{M_{Tx}}[m]]^T$ contains the symbols transmitted from M_{Tx} transmit antennas at time m. Similarly, the corresponding received vector is represented by $\mathbf{y}[m] = \left[y_1[m], y_2[m], \cdots, y_{M_{Rx}}[m]\right]^T$ where for a single tap channel,

$$\mathbf{y}[m] = \mathbf{H}[m]\mathbf{x}[m] + \mathbf{z}[m]. \tag{3.2}$$

$\mathbf{H}[m]$ is the $M_{Rx} \times M_{Tx}$ channel matrix and $\mathbf{z}[m]$ is the corresponding additive white Gaussian noise vector at time m. The received vector, $\mathbf{y}[m]$, is first multiplied by the combiner matrix $\mathbf{G}[m]$ and then is processed for data detection.

Precoder and combiner matrices are designed to make decoupling of data steams possible at the receiver. To avoid performance degradation, the precoder and com-

biner should be matched to the channel matrix. The optimal precoder and combiner can be obtained from the eigenvectors of the channel matrix [34]. For the slow time-varying channels, the precoder matrix $\mathbf{F}[m]$ is considered to be constant over each frame, i.e., for $m \in \mathbb{I}_{M_f}$. So, it can be calculated once based on the estimated channel matrix at the beginning of each frame. The precoder matrix, is then fed back to the transmitter directly in infinite feedback rate systems or it is first quantized based on a predefined codebook and the quantization index is fed back in finite feedback rate systems. The same precoder will be used through the whole frame. However, in fast time-variant channels, $\mathbf{F}[m]$ becomes out of date very quickly and it is required to be updated even inside one frame which is impossible due to channel estimation and feedback delays. To overcome the feedback delay problem, it is proposed to pr edict the channel coefficients and design the precoder in advance [36], [37]. In the next section we will investigate two channel prediction schemes which can be used for precoder design in fast time-variant channels.

Note that, here after, $h_{k,l}[m]$ represents the channel impulse response for (k,l)-antenna pair at time m. Moreover, we consider independent and identically distributed (i.i.d.) Rayleigh fading channel based on the Jakes' model for each antenna pair with no spatial correlation between different antennas as in [61].

3.3 AR and ME Channel Predictors

In this section a brief introduction to ME and AR channel predictors is presented which then will be used for introducing the proposed DPS-AR channel predictor in the next section.

3.3.1 ME Channel Predictor

A low complexity ME channel predictor is proposed in [60] which is based on a subspace spanned by time-concentrated and band limited DPS sequences and it is shown that for a fading process with constant spectrum over its support the ME

predictor is identical to a reduced-rank maximum-likelihood predictor.

For (k,l)-antenna pair, the ME predictor uses the band-limitation of the fading channel and models the channel over the first M known coefficients of each frame as a linear combination of D_t dominant DPS basis

$$h_{k,l}[m] = \sum_{i=0}^{D_t-1} u_i[m,W,M]\psi_i^{k,l} \quad for \quad m \in \mathbb{I}_M \tag{3.3}$$

where D_t is the essential dimension of the subspace spanned by DPS sequences and is given by [62],

$$D_t(W,M) = \lceil |W|M \rceil + 1. \tag{3.4}$$

with $|W| = 2f_dT_s$ indicating the maximum normalized support of the signal in frequency domain. For a highly oversampled fading process $|W| \ll 1$ and the process can be approximated by $D_t(W,M) \ll M$ DPS basis which reduces the amount of computational complexity. The basis coefficients $\{\psi_i^{k,l}\}_{i=0}^{D_t-1}$ are estimated as

$$\Psi_{k,l} = \mathbf{U}^H \boldsymbol{h}_{k,l} \tag{3.5}$$

where $\mathbf{h}_{k,l} = [h_{k,l}[0], \cdots, h_{k,l}[M-1]]^T$ contains the know channel coefficients, $\Psi_{k,l} = [\psi_0^{k,l}, \cdots, \psi_{D_t-1}^{k,l}]^T$ and $[\mathbf{U}]_{m,i} = u_i[m,W,M]$ for $m \in \mathbb{I}_M$ and $i \in \mathbb{I}_{D_t}$.

In the ME predictor, the estimated basis coefficients from (3.5) are used for predicting the future channel coefficients by extrapolating the DPS basis $\{u_i[m,W,M]\}_{i=0}^{D_t-1}$ over $m = M, \cdots, M_f - 1$ based on (2.15) and using the same linear combination of the extrapolated basis presented in (3.3). As the DPS sequences are most energy concentrated in $\mathbb{I}_M$, among the infinitely many ways for extending the band-limited channel samples over $m \in \mathbb{Z} \setminus \mathbb{I}_M$, the ME predictor is the only one that extends the channel in an ME continuation sense [60].

3.3.2 AR Channel Predictor

Comparing different channel prediction algorithms, it is concluded in [63] that the AR model based predictors, known as Wiener predictors [64], outperform the PRC model based schemes both for synthesized and measured radio channels at least for the narrowband case. Assuming the channel is known over the first M samples of each frame, the Wiener predictor predicts the channel at $m \in \{M, \cdots, M_f - 1\}$ using the weighted linear combination of the M most recent channel coefficients as follows:

$$\hat{h}_{k,l}[m] = \mathbf{w}_{k,l}[m]^H \tilde{\mathbf{h}}_{k,l}[m] \tag{3.6}$$

where $\mathbf{w}_{k,l}[m]$ is the $M \times 1$ weighting vector and $\tilde{\mathbf{h}}_{k,l}[m]$ is defined as

$$\tilde{\mathbf{h}}_{k,l}[m] = \left[\hat{h}_{k,l}[m-1], \hat{h}_{k,l}[m-2], \cdots, \hat{h}_{k,l}[m-M]\right]^T \tag{3.7}$$

which we call it the history vector with $\hat{h}_{k,l}[m']$ being the known channel coefficient for $m' \in \{0, \cdots, M-1\}$ and the previously predicted channel coefficient for $m' \in \{M, \cdots, M_f - 1\}$. The weighting vector $\mathbf{w}_{k,l}[m]$ is obtained through minimizing the mean square error (MSE) between the predicted channel and real channel at time m,

$$\mathbf{w}[m] = \underset{\mathbf{w}}{\operatorname{argmin}}\, \mathbb{E}\left\{ \parallel h[m] - \mathbf{w}[m]^H \tilde{\mathbf{h}}[m] \parallel^2 \right\} \tag{3.8}$$

which leads to

$$\mathbf{w}[m] = \mathbf{R}_{hh}[m]^{-1} \mathbf{r}_{hh}[m] \tag{3.9}$$

and the $M \times M$ matrix $\mathbf{R}_{hh}$ and the $M \times 1$ vector $\boldsymbol{r}_{hh}$ are defined as

$$\begin{aligned} [\mathbf{R}_{hh}[m]]_{i,j} &= \mathbb{E}\left\{h[m-i]h^*[m-j]\right\} \\ [\boldsymbol{r}_{hh}[m]]_j &= \mathbb{E}\left\{h[m]h^*[m-j]\right\} \text{ for } i, j = 1, \cdots, M \end{aligned} \tag{3.10}$$

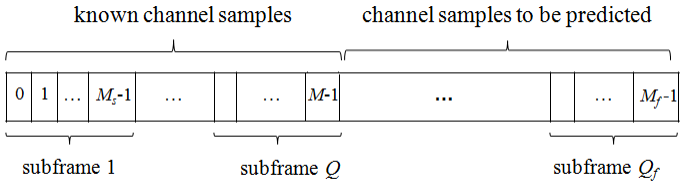

Figure 3.2: Transmitted frame structure for each antenna

Note that for notation simplicity, the antenna pair index (k, l) is omitted in (4.8)-(4.11) and in the rest of this chapter.

3.4 Proposed DPS-AR predictor

In this section a new DPS based AR (DPS-AR) channel predictor will be presented which takes the advantage of the low computational complexity induced by the DPS sequences and the performance gain of AR model, simultaneously. We will also investigate the application of the proposed scheme for the precoder design in time-variant channels.

3.4.1 DPS-AR channel predictor

Consider the transmitted frame over each antenna is divided into Q_f subframes of $M_s = M_f/Q_f$ length shown in Fig. 3.2. The first $Q = M/M_s$ subframes contain the M known channel samples, and the channel coefficients of the rest of $Q_f - Q$ subframes are to be predicted. We use the DPS sequences to model the channel's time-variation inside each subframe. It is clear from (2.15) that for each subframe the DPS basis depend on the length of the subframe and the normalized Doppler spread of the channel. Considering the same maximum Doppler frequency over the whole frame and the same length for all subframes, the DPS basis would be the same for all subframes and only the basis coefficients would change from one subframe to another one. Using D_s dominant DPS basis, the channel impulse response inside the

qth subframe can be approximated as follows for each antenna pair,

$$h[(q-1)M_s+m] \approx \sum_{i=0}^{D_s-1} u_i[m,W,M_s]\psi_i[q] \quad for \quad m \in \mathbb{I}_{M_s} \tag{3.11}$$

where m indicates the mth sampling time inside each subframe and $\psi_i[q]$ is the ith basis coefficient for subframe q.

As mentioned previously, the basis $\{u_i[m,W,M_s], i \in \mathbb{I}_{D_s}, m \in \mathbb{I}_{M_s}\}$ are independent of q and they are the same for all subframes. So for tracking the time-variation of the channel, we only require to track the changes of the basis coefficients $\{\psi_i[q]\}_{i=0}^{D_s-1}$ over adjacent subframes. In order to predict the basis coefficients for future subframes we will use the AR model. For the qth subframe, the ith basis coefficient, $\psi_i[q]$, is predicted from,

$$\hat{\psi}_i[q] = \mathbf{w}_i[q]^H \tilde{\Psi}_i[q] \tag{3.12}$$

where $\tilde{\Psi}_i[q]$ is a $Q \times 1$ history vector which contains the ith coefficient of the Q recent predicted/known subframes and is defined as

$$\tilde{\Psi}_i[q] = \left[\hat{\psi}_i[q-1], \cdots, \hat{\psi}_i[q-Q]\right]^T \tag{3.13}$$

Using the same idea as (3.8), the MMSE weighting vector $\boldsymbol{w}_i[q]$ is obtained from

$$\mathbf{w}_i[q] = \mathbf{R}_i[q]^{-1}\mathbf{r}_i[q] \tag{3.14}$$

where

$$[\mathbf{R}_i[q]]_{k,l} = \mathbb{E}\left\{\psi_i[q-l]\psi_i^*[q-k]\right\} \qquad \text{for } k,l = 1,...,Q \tag{3.15}$$

and

$$\boldsymbol{r}_i[q] = \left[\mathbb{E}\left\{\psi_i[q]\psi_i^*[q-1]\right\}, \mathbb{E}\left\{\psi_i[q]\psi_i^*[q-2]\right\}, \cdots, \mathbb{E}\left\{\psi_i[q]\psi_i^*[q-Q]\right\}\right]^T \tag{3.16}$$

with $\mathbb{E}\{\psi_i[q]\psi_i[q']\}$ indicating the amount of the correlation between the ith basis coefficient of the qth and q'th subframes. For estimating the correlation between the basis coefficients of different subframes we can write the following vector-matrix relationship for the qth subframe based on (3.11) and by considering $D_s = M_s$,

$$\mathbf{h}[q] = \mathbf{U}_t \Psi_t[q] \tag{3.17}$$

where $\mathbf{U}_t$ is an $M_s \times M_s$ matrix with $[\mathbf{U}_t]_{m,i} = u_i[m, W, M_s]$ for $m, i \in \mathbb{I}_{M_s}$, $\mathbf{h}[q]$ contains the channel coefficients of the qth block with $[\mathbf{h}[q]]_m = h[(q-1)M_s + m]$ and $[\Psi_t[q]]_i = \psi_i[q]$. Multiplying both sides of (3.17) by their hermitian at q' and taking the expectation of them the following relationship is obtained between the correlation function of the channel and the correlation function of the basis coefficient between the qth and q'th subframes,

$$\mathbf{R}_{\Psi_t}[q, q'] = \mathbf{U}_t^H \mathbf{R}_{\mathbf{h}}[q, q'] \mathbf{U}_t \tag{3.18}$$

where $\mathbf{R}_{\Psi_t}[q, q'] = \mathbb{E}\{\Psi_t[q]\Psi_t[q']^H\}$ and $\mathbf{R}_{\mathbf{h}}[q, q'] = \mathbb{E}\{\mathbf{h}[q]\mathbf{h}[q']^H\}$. Note that for a stationary channel $\mathbf{R}_{\mathbf{h}}[q, q'] = \mathbf{R}_{\mathbf{h}}[q - q']$ and consequently $\mathbf{R}_{\Psi_t}[q, q'] = \mathbf{R}_{\Psi_t}[q - q']$ which results in the same $\mathbf{w}_i[q]$ for different value of q.

3.4.2 Mean Square Error of the Predictor

As it is discussed in the previous section, the channel inside each subframe is modelled by D_s DPS basis and each basis coefficient is predicted using a Q-order AR model. So the predicted channel impulse response of the qth subframe is modelled as,

$$\hat{\mathbf{h}}[q] = \mathbf{U}_{D_s} \hat{\Psi}_{D_s}[q] \tag{3.19}$$

where $\mathbf{U}_{D_s}$ is an $M_s \times D_s$ matrix containing the first D_s dominant DPS basis as its columns and $\hat{\Psi}_{D_s}[q]$ is a $D_s \times 1$ vector containing the corresponding predicted basis coefficients at the qth subframe which differs from the original basis coefficient vector

$\Psi_{D_s}[q]$ by the AR prediction error vector $\mathbf{e}_{AR}[q]$ as follows

$$\hat{\Psi}_{D_s}[q] = \Psi_{D_s}[q] + \mathbf{e}_{AR}[q] \quad \text{for} \quad q = Q+1, \cdots, Q_f \tag{3.20}$$

where

$$[\mathbf{e}_{AR}[q]]_i = \hat{\psi}_i[q] - \psi_i[q] = \underbrace{\mathbf{w}_i[q]^H \Psi_i[q] - \psi_i[q]}_{e_M[q,i]} + \underbrace{\mathbf{w}_i[q]^H \mathbf{e}_i[q]}_{e_P[q,i]} \quad \text{for} \quad i = 1, 2, \cdots, D_s. \tag{3.21}$$

In (3.21) $\hat{\psi}_i[q]$ is replaced by $\mathbf{w}_i[q]^H \tilde{\Psi}_i[q]$ according to (4.31) and the error contribution from the previously predicted coefficients, resulting in the so-called AR propagation error $e_P[q,i]$, is reflected in the $Q \times 1$ vector $\mathbf{e}_i[q] = \tilde{\Psi}_i[q] - \Psi_i[q]$ with $[\mathbf{e}_i[q]]_j = [\mathbf{e}_{AR}[q-j]]_i$ being its jth element. $e_M[q,i]$ is called the AR modelling error which is the result of the prediction in an MMSE sense using the MMSE weighting vector $\mathbf{w}_i[q]$.

Using (3.17), (3.19) and (3.20), the mean square error of the qth block is defined as,

$$\text{MSE}[q] = \mathbb{E}\left\{ \| \mathbf{h}[q] - \hat{\mathbf{h}}[q] \|^2 \right\} = \underbrace{\mathbb{E}\left\{ \| \mathbf{V}^H \mathbf{h}[q] \|^2 \right\}}_{\text{MSE}_{\text{DPS}}[q]} + \underbrace{\mathbb{E}\left\{ \| \mathbf{e}_{AR}[q] \|^2 \right\}}_{\text{MSE}_{\text{AR}}[q]} \tag{3.22}$$

where in deriving (3.22) we used the fact that the DPS basis are orthonormal and independent of the AR prediction error and $\mathbf{V} = [\mathbf{u}_{Ds}, ..., \mathbf{u}_{M_s-1}]$ contains the $M_s - D_s$ less dominant DPS basis spanning the subspace orthogonal to the signal subspace spanned by columns of $\mathbf{U}_{D_s}$. $\text{MSE}_{\text{DPS}}[q]$ is the mean square of DPS reconstruction error caused by using the limited number of basis for modelling the channel inside each subframe which according to (3.18) can be simplified to,

$$\text{MSE}_{\text{DPS}}[q] = \sum_{i=D_s}^{M_s-1} \mathbf{u}_i^H \mathbf{R}_{\mathbf{h}}[q,q] \mathbf{u}_i = \sum_{i=D_s}^{M_s-1} \mathbb{E}\{|\psi_i[q]|^2\} \tag{3.23}$$

where for a stationary channel $\mathrm{MSE}_{\mathrm{DPS}}[q]$ is independent of the subframe index q. Using (3.21), $\mathrm{MSE}_{\mathrm{AR}}[q]$ can be also obtained from,

$$\mathrm{MSE}_{\mathrm{AR}}[q] = \sum_{i=0}^{D_s-1} \mathbb{E}\left\{|[\mathbf{e}_{AR}[q]]_i|^2\right\} = \sum_{i=0}^{D_s-1} \mathbb{E}\left\{|e_M[q,i] + e_P[q,i]|^2\right\} \quad (3.24)$$

It is clear that for a given normalized channel bandwidth W, $\mathrm{MSE}_{\mathrm{DPS}}[q]$ and $\mathrm{MSE}_{\mathrm{AR}}[q]$ can be controlled by the subframe length M_s and the number of DPS basis per subframe D_s. While increasing the number of basis would decrease $\mathrm{MSE}_{\mathrm{DPS}}[q]$, it would increase the AR prediction error since more coefficients are required to be predicted. As for the subframe length, choosing M_s to be too small would increase the AR modelling error as the history vector is more correlated specifically for low Doppler frequencies which can result in a rank deficient matrix $\mathbf{R}_i[q]$ in (3.14) and less accurate weighting vector $\mathbf{w}_i[q]$ estimation. Smaller subframe length also increases the number of subframes to be predicted which can lead to a bigger AR propagation error. On the other hand, very large subframe length may also increase the AR modelling error due to the increased distance between the history samples which may not be correlated enough with the basis coefficient to be predicted especially in fast time variant channels.

So for the normalized bandwidth W and M known channel coefficients at the beginning of each frame, the subspace dimension and the subframe length which minimize the total MSE over the frame of length M_f with Q_f subframes can be obtained from the following optimization problem,

$$[M_s^{opt}(W), D_s^{opt}(W)] = \underset{\substack{M_s \text{is a factor of } M \\ D_s \in \{1,2,\ldots,M_s\}}}{\operatorname{argmin}} \left(\sum_{q=Q+1}^{Q_f} \sum_{i=D_s}^{M_s-1} \mathbb{E}\{|\psi_i[q]|^2\} + \sum_{q=Q+1}^{Q_f} \sum_{i=0}^{D_s-1} \mathbb{E}\left\{|e_M[q,i] + e_P[q,i]|^2\right\} \right). \quad (3.25)$$

For solving (3.25) we can use Algorithm 1 which usually converges after two or three

iterations.

Algorithm 1 Algorithm for calculating $M_s^{opt}(W)$ and $D_s^{opt}(W)$

Input: M, M_f, W

Output: $M_s^{opt}(W)$, $D_s^{opt}(W)$

Initialisation : $k = 1$, $M_s(k) = M$

1: $Q = \frac{M}{M_s(k)}$, $Q_f = \frac{M_f}{M_s(k)}$

2: Find $D_s(k) \in \{1, \cdots, M_s(k)\}$ which minimizes (3.25)

3: $k \leftarrow k + 1$

4: $D_s(k) \leftarrow D_s(k-1)$

5: Find $M_s(k) \in \{m | m \text{ is a factor of } M \text{ and } m \geq D_s(k)\}$ which minimizes (3.25)

6: **while** $M_s(k) \neq M_s(k-1)$ **do**

7: $\quad k \leftarrow k + 1$

8: $\quad M_s(k) \leftarrow M_s(k-1)$

9: $\quad$ Repeat 1 to 5

10: **end while**

11: **return** $M_s^{opt}(W) = M_s(k)$ and $D_s^{opt}(W) = D_s(k)$

Assuming $M = 30$ and $M_f = 120$, Table 3.1 shows the optimum values of M_s, D_s and the corresponding value of $Q = M/M_s$, for different normalized Doppler frequencies. It is clear that by increasing the maximum normalized Doppler frequency the optimal subframe length decreases and the ratio of D_s/M_s increases. In fact when the channel varies more rapidly, the correlation between the basis coefficients of different subframes will decrease which requires smaller subframe length for reducing the AR prediction error. Moreover, to reduce the DPS reconstruction error at high Doppler frequencies more DPS basis per subframe are required for better tracking of the time-variation of the channel in each subframe.

Table 3.1: Optimal subframe length and subspace dimension for $M = 30$ and $M_f = 120$

Normalized Doppler Frequency ($f_d T_s$)	0.001	0.002	0.005	0.01	0.015	0.02
M_s	10	10	6	6	6	5
D_s	3	3	3	3	3	3
Q	3	3	5	5	5	6

For different normalized Doppler frequencies and the optimum values of Table 3.1, Fig. 3.3 shows the AR prediction mean square error for each of the basis coefficients as well as the DPS reconstruction mean square error for each subframe $q \in \{Q+1, \cdots, Q_f\}$ over the prediction length of $M_f - M = 90$ channel samples. As expected, by increasing the Doppler frequency, the amount of different types of error will increase. Moreover, since the simulated channel is wide sense stationary the DPS reconstruction error is constant over different subframes and the small amount of $\mathrm{MSE}_{\mathrm{DPS}}[q]$ indicates the proper performance of the time variation modelling of the channel inside each subframe using adequate number of DPS basis. As for the AR prediction error, it is clear the less dominant basis have smaller prediction error as they have less contribution in channel modelling (have smaller basis coefficients).

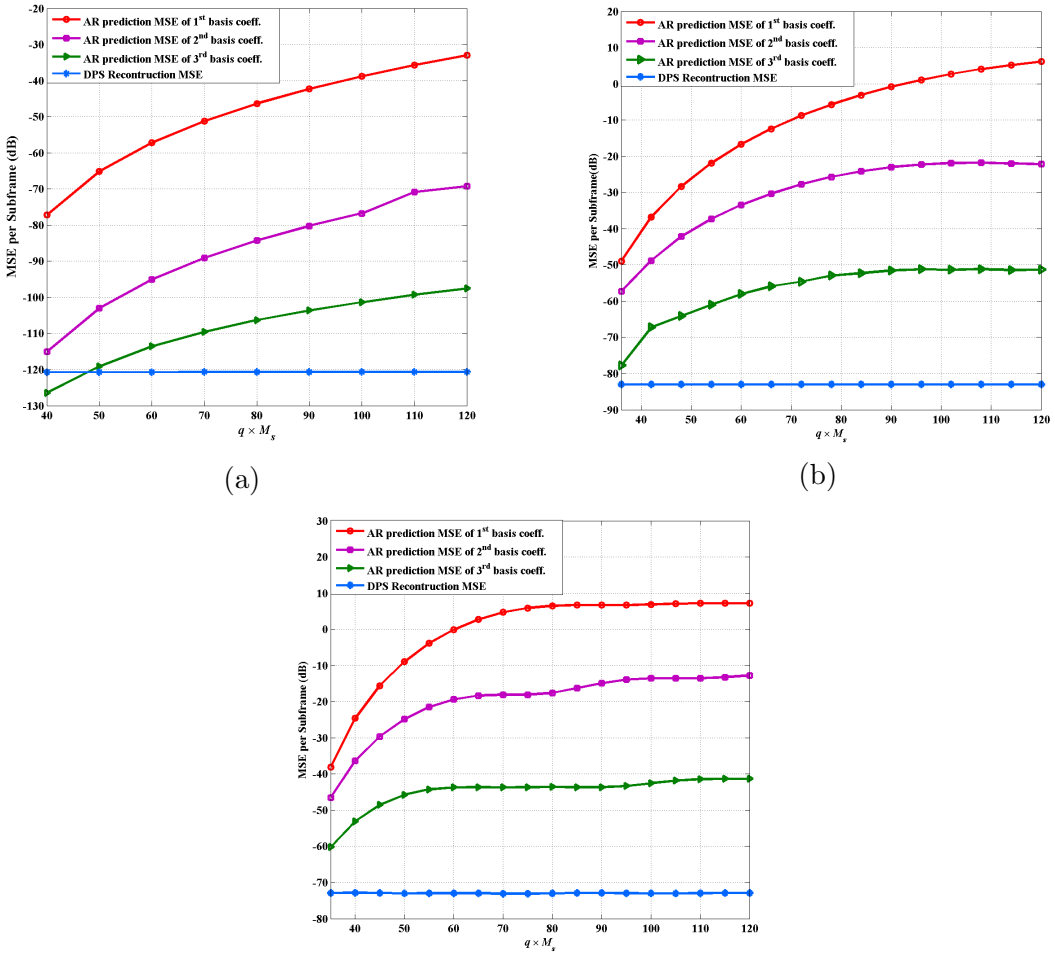

Figure 3.3: Basis coefficients' AR prediction error and DPS modelling error per each subframe $q \in \{Q+1, \cdots, Q_f\}$ over the prediction length of $M_f - M = 120 - 30 = 90$ channel samples for (a) $f_d T_s = 0.001, M_s = 10, Q = 3, Q_f = 12$, (b) $f_d T_s = 0.01, M_s = 6, Q = 5, Q_f = 20$, (c) $f_d T_s = 0.02, M_s = 5, Q = 6, Q_f = 24$.

For evaluating the prediction quality of the proposed scheme over the samples of each subframe, we can also calculate the amount of error at the mth sample of the qth subframe as follows,

$$\begin{aligned} e[q,m] &= h[(q-1)M_s + m] - \hat{h}[(q-1)M_s + m] \\ &= \underbrace{h[(q-1)M_s + m] - \sum_{i=0}^{D_s-1} u_i[m]\psi_i[q]}_{e_{DPS}[m]} \underbrace{- \sum_{i=0}^{D_s-1} u_i[m]\,[\mathbf{e}_{AR}[q]]_i}_{e_{AR}[m]} \end{aligned} \tag{3.26}$$

where $e_{DPS}[m]$ and $e_{AR}[m]$ are associated with the DPS modelling error and the AR prediction error of different basis coefficients, respectively. As discussed, the error contribution from the DPS modelling is fairly small and it can be concluded that the error at each sample is mainly controlled by the second term which is a linear combination of the AR prediction error of different basis coefficients weighted by the corresponding DPS basis values at time m. Since the DPS basis may not be all strictly ascending or descending functions over the subframe length and can take both positive and negative values, the error at each sample inside each subframe can follow an increasing, decreasing or even constant trend due to constructive or destructive contribution from the weighted prediction error of different basis coefficients. Fig. 3.4 indicates the error per sample for different normalized Doppler frequencies and the optimal values of Table 3.1.

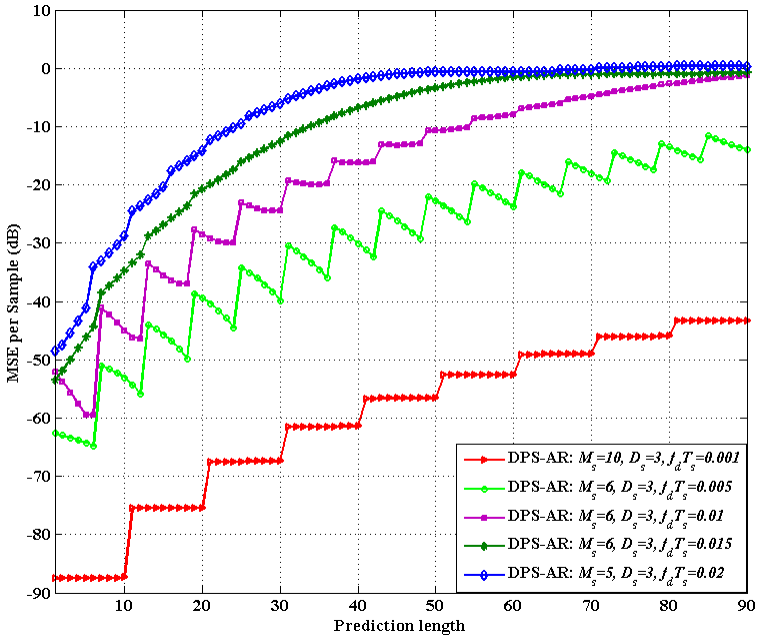

Figure 3.4: MSE of the proposed DPS-AR prediction scheme over 90 channel samples

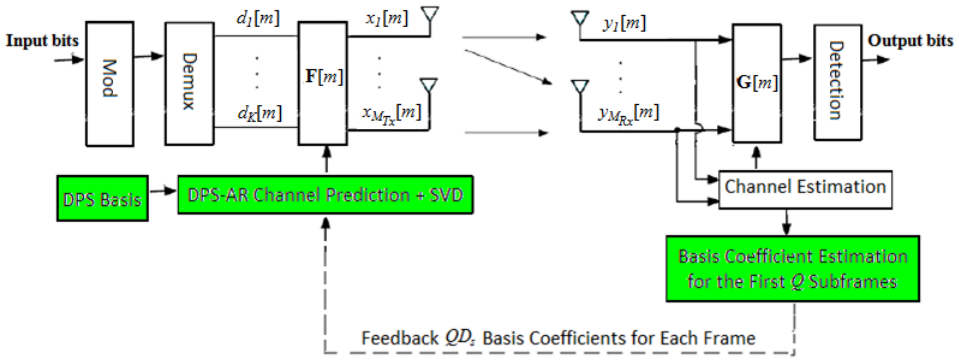

Figure 3.5: Proposed precoded MIMO system

3.4.3 Application to Precoder Design

The DPS-AR channel predictor which is proposed in the previous section can be used to reduce the feedback load and the feedback delay of sending the CSI to the transmitter for precoder design in time-variant channels. Based on the proposed scheme shown in Fig. 3.5, it is only required to feedback the D_s basis coefficients of the first Q known/estimated subframes for predicting the channel and designing the precoder over the subsequent subframes of each frame. The relative amount of feedback load reduction compared to the case of sending back the channel impulse response of the first M samples of each frame is in the order of $F_R = O(\frac{M_s}{D_s})$ per each antenna pair. Based on the optimum values of M_s and D_s presented in Table 3.1, the proposed DPS-AR predictor offers significant feedback load reduction specially for slower time-variant channels and massive MIMO systems. Fig. 3.6 shows the amount of feedback load reduction for different antenna sizes.

It should be also noted that, the DPS sequences are the same for different subframes and can be calculated once and stored at the transmitter based on the known maximum normalized Doppler frequency and the chosen subframe length. Once the channel is predicted for each subframe the precoder can be obtained using the SVD decomposition of the channel matrix.

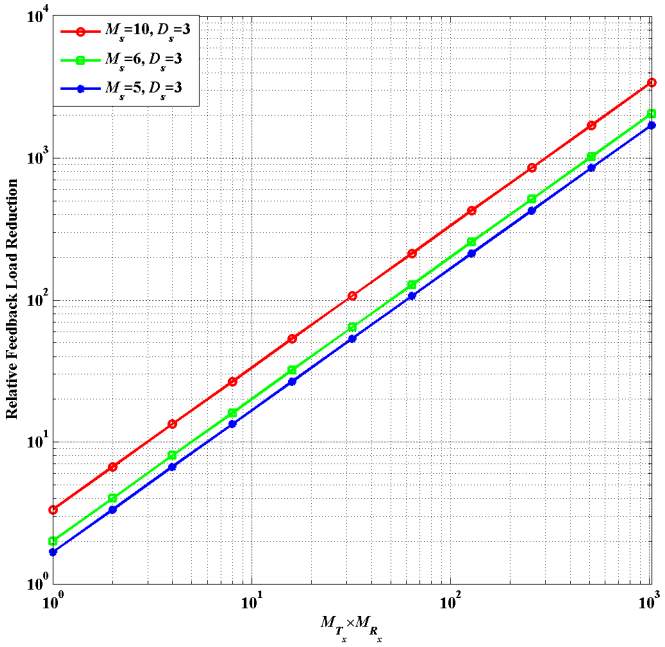

Figure 3.6: Relative feedback load reduction for different MIMO sizes

3.5 Simulation Results

In this section the performance of the proposed DPS-AR channel predictor is compared with that of the AR and the ME channel predictors. Fig. 3.7 shows the normalized MSE (NMSE) for different prediction schemes at the prediction length p which is defined as,

$$\text{NMSE}[p] = \frac{1}{p} \sum_{m=M+1}^{M+p} \mathbb{E}\{|h[m] - h_{pre}[m]|^2\} \tag{3.27}$$

where $h_{pre}[m]$ is the predicted channel sample at time m. As it is expected the ME predictor has lower accuracy both for low and high maximum normalized Doppler frequencies compared to the proposed DPS-AR predictor. This is due to the fact that ME predictor assumes that most of the energy of the channel is contained in the known samples at the beginning of each frame and extends the channel over the future time instants in an ME continuation sense which has a low complexity but

would not guarantee the best prediction accuracy for the signals that do not have low energy over their prediction interval. The proposed predictor also outperforms the AR approach for low to medium normalized Doppler frequencies and it has almost the same performance as the AR method for high normalized Doppler frequencies. The reason for that is the fact that in lower Doppler frequencies, the history vector in the AR predictor contains more correlated samples resulting in inaccurate weighting vector estimation. However, for the proposed DPS-AR scheme the basis coefficients are sampled far enough from each other based on the selected subframe length which increases the accuracy of the weighting vector estimation and reduces the AR prediction error of the basis coefficients. On the other hand, by proper selection of the number of basis the DPS reconstruction error is controlled to be small enough and consequently the total prediction error of the proposed DPS-AR scheme would be smaller than that of the AR model. Increasing the Doppler frequency, however reduces the correlation in the history vector of the AR predictor leading AR predictor to reach its best performance and reduces the gap between the two schemes.

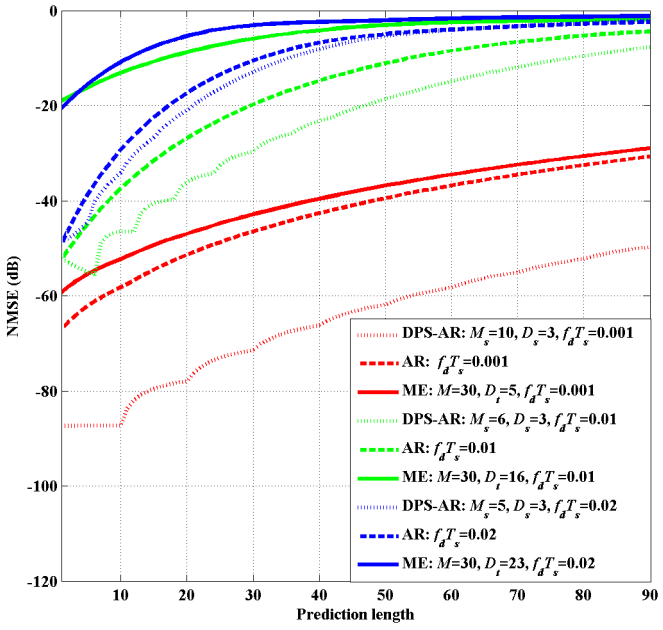

Figure 3.7: NMSE comparison of different predictors at different prediction length and for different Doppler frequencies

In terms of the computational complexity it is clear from (3.9) and (3.14) that the conventional AR method requires calculating an M-order MMSE filter, $\mathbf{w}[m]$, for each $m \in \{M, \cdots, M_f - 1\}$, while the proposed scheme requires to calculate a Q-order MMSE filter, $\mathbf{w}_i[q]$, for each $i \in \{0, \cdots, D_s - 1\}$ and each $q \in \{Q+1, \cdots, Q_f\}$. The computational complexity of the MMSE filter for the conventional AR model is in the order of $C_{AR} = O(M^3(M_f - M))$ and for the proposed reduced rank DPS-AR scheme is in the order of $C_{DPS-AR} = O(D_s Q^3 \frac{M_f - M}{M_s})$. Fig. 3.8 shows the relative amount of computational complexity reduction $C_R = C_{AR}/C_{DPS-AR} = M_s^4/D_s$ for different MIMO sizes. So, although for more fast time variant channels the DPS-AR method has almost the same performance as the AR predictor, it still outperforms the AR method in terms of the computational complexity.

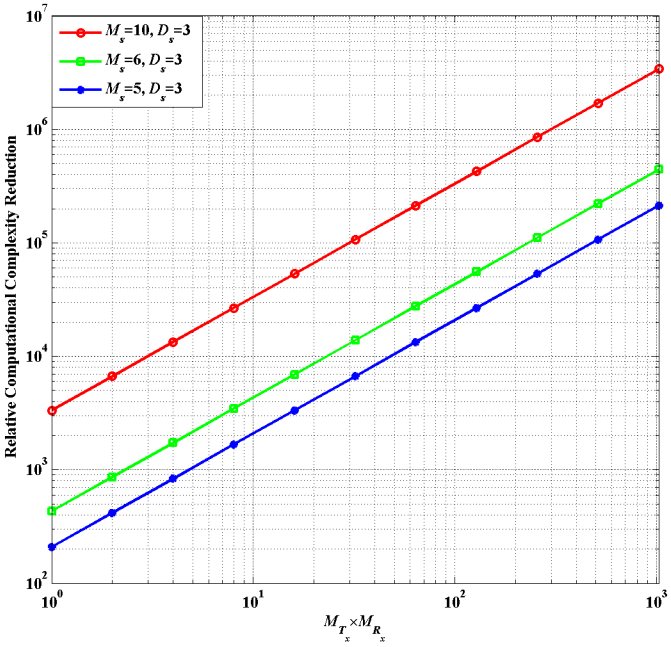

Figure 3.8: Relative computational complexity reduction for different MIMO sizes

3.6 Conclusion

In this chapter we have proposed a low complexity channel predictor which uses the DPS basis in combination with an AR model to track the channel's time varia-

tion. The same DPS basis are used to model the time-variant channel inside different subframes and the AR model is used for tracking the time variation of the basis coefficients in each transmitted frame. The subframe length and the number of DPS basis used for channel modelling in each subframe are obtained by minimizing the MSE of the proposed predictor and it is shown that the bigger the normalized Doppler frequency is, the smaller should be the sub-frame length and the bigger should be the number of basis per subframe. The simulation results demonstrates the better prediction accuracy of the DPS-AR scheme in comparion to the ME predictor for different prediction length and different ranges of maximum normalized Doppler frequency. Moreover, comparing to AR predictor the DPS-AR approach has better performance both in terms of computational complexity and MSE for low to moderate time variant channels and has almost the same performance for fast time variant channels with lower complexity. The proposed channel predictor can be applied for predicting the precoder in time varying MIMO channels with reduced amount of the required feedback load.

Chapter 4

Hybrid mm-Wave MIMO-OFDM Channel Estimation Based on the Multi-Band Sparse Structure of Channel

4.1 Introduction

The potential availability of large bandwidth channels at mm-wave frequencies and the small wavelength of the mm-waves, offer the mm-wave massive MIMO communication as a promising technology for 5G cellular networks which enables Giga-bit-per second data rates [65]. Due to the high fabrication cost and power consumption of the RF units at mm-wave frequencies, hybrid analog/digital architectures, which use a small number of RF chains and divide the precoding/combining processing between RF and baseband domains are proposed for efficient implementation of mm-wave massive MIMO systems [66, 67, 68]. The hardware constraint of the hybrid architecture makes the mm-wave channel estimation a challenge [69].

Exploiting the sparse nature of mm-wave channel in the angular domain, the

channel estimation problem can be solved within the compressed sensing (CS) framework [66], [70, 71, 72, 73]. In the CS formulation the equivalent measurement matrix consists of the dictionary matrix which contains fixed basis functions to exploit the sparsity of the channel and the training precoder/combinder vectors which are designed to minimize the coherence of the measurement matrix for unique recovery of the sparse channel [69]. Discrete spatial Fourier transform (DSFT) basis or the antenna array response vectors can be used as the columns of the dictionary matrix to obtain a sparse channel representation known as the virtual [74, 75, 76] or extended virtual channel model [69], respectively.

In the virtual channel representation the number of DSFT basis used for obtaining the sparse angular spectrum equals to the number of Tx/Rx antennas which limits the angular resolution. Moreover, based on the Fourier transform properties the limited antenna array length causes power leakage problem in the angular spectrum and decreases the sparsity level of the channel [66]. Paper [77] tries to improve the angular resolution by using a redundant dictionary containing much more uniform DSFT basis than the number of antennas. Increasing the number of DSFT basis, however, is equivalent to sampling the angular spectrum at a higher rate which will increase both the length of the sparse angular channel vector required to be recovered and the number of nonzero elements of it. So, more channel measurements (longer training sequences) should be obtained for unique recovery of the signal [78, 79].

The extended virtual channel representation considers a parametric channel model where the AOAs/AODs are assumed to be taken from a quantized angle grid distributed uniformly over $[0, 2\pi]$ and the columns of the measurement matrix are the array response vectors corresponding to these angles [69]. The sparse channel vector length is determined by the angle grid size and the sparsity level of the channel vector equals to the number of multi-path components which is smaller than that of the virtual channel model both with conventional or redundant dictionary matrices and correspondingly smaller number of measurements are required for CS channel estimation. However, since in the extended virtual channel model the angles are chosen

from a uniform grid, the array response vectors (columns of the dictionary matrices) may not be orthogonal which increases the coherency of the equivalent measurement matrix and degrades the CS reconstruction accuracy compared to the virtual channel model with orthogonal DSFT basis [77]. Since the AOAs/AODs are continuous, it is clear that for both the virtual and extended virtual channel models the angle quantization error may only be neglected if the number of dictionary basis tends to infinity which is impossible. Adaptive design of the dictionary matrix is proposed in [80] and [81] for narrowband and broadband massive MIMO systems, respectively. In these adaptive schemes a multi-stage procedure is applied which uses coarse angle grids in the first stage to obtain a rough estimate of AOAs/AODs using CS recovery algorithms and improves the estimation by refining the grids iteratively around the estimated angles in the next stages.

Beside different possible sparse channel models, different hybrid architecture have also been proposed based on the traditional random CS tools [70, 71, 72, 81] or adaptive CS techniques [66] where the RF precoders/combiners can be implemented using networks of random/fixed phase shifters [68], [82], lens antennas [83, 84] and/or low power switches [73, 85].

In this chapter we develop a new power efficient CS-based mm-wave channel estimation scheme for hybrid MIMO-OFDM systems. The proposed channel estimator addresses the limited angular resolution problem through recovering the continuous instead of discretized angular spectrum and also considers the power leakage issue by modeling the angular channel as a multi-band signal with the number of sub-bands being equal to the number of multi-path components and the bandwidth of each being controlled by the antenna array length. Our channel estimation approach is adapted from the spectrum blind reconstruction of the multi-band signals at minimal sampling rates [86] and the proposed hybrid architecture is based on switches to further reduce the complexity and power consumption of the RF combiner.

Contributions:

1. We formulate the sparse MIMO-OFDM mm-wave channel estimation problem

based on the multi-band structure of the continuous angular channel and a multi-coset sampling pattern for antenna subset selection. The CS formulation considers multiple measurement vectors (MMV) and the same sparsity structure of the sub-carriers for the joint recovery of the channels of all sub-carriers. In the proposed multi-band MMV (MB-MMV) approach the angular channel is treated in the continuous framework and the angular support is recovered using a finite dimensional problem without any discretization. So, unlike the previous discrete channel models for which the number of measurements is controlled by the desired angular resolution (grid size), for the proposed scheme the number of measurements only depends on the number of channel's paths and the bandwidth of each sub-band.

2. The proposed MB-MMV channel estimator is implemented using a hybrid architecture made up of a network of switches for RF combiner design and a baseband processor. The proposed hybrid scheme is analysed in terms of minimum number of required RF chains and the RF power consumption and the system performance is evaluated for different system parameters using Monte Carlo simulation.

4.2 System Model

We consider a mm-wave massive MIMO-OFDM system with K_u single antenna users and a base station (BS) equipped with a uniform linear antenna array of N_{BS} antennas. The number of RF chains at the BS is N_{RF} and each user has a single RF chain. For estimating the channel of the kth user we assume that while other users are silent, an OFDM symbol of P sub-carriers with the cyclic prefix length of L_{CP} is sent from this user. The continuous spatial domain channel of the kth user at the

pth sub-carrier is modelled as,

$$h_k(\hat{s},p)=\sum_{l=0}^{L_k-1}\alpha_{l,k}e^{-j2\pi p f_s\tau_{l,k}/P}e^{j2\pi\hat{s}\sin(\theta_{l,k})/\lambda}\qquad \hat{s}\in(-\infty,+\infty)\qquad(4.1)$$

where f_s is the frequency bandwidth leading to adjacent sub-carrier distance of f_s/P, λ is the signal wavelength, L_k is the number of paths and $\alpha_{l,k}$, $\tau_{l,k}$ and $\theta_{l,k}$ are the complex gain, delay and AOA of the lth path of user k, respectively. The channel at the sth receive antenna, $h_k[s,p]$, is obtained by sampling $h_k(\hat{s},p)$ at $\hat{s}=sd$ where d is the distance between the adjacent antennas.

If $L_{CP}\geq\max(\tau_{l,k})$ and each of the receive antennas at the BS is equipped with one RF chain, i.e., $N_{RF}=N_{BS}$, then the received signal from the kth user is modelled as,

$$x_k[s,p]=h_k[s,p]d_k[p]+z_k[s,p]\qquad(4.2)$$

where $d_k[p]$ is the pilot symbol sent at the sub-carrier p of user k and for channel estimation we can assume binary pilots, i.e., $d_k[p]=1$. z_k is the corresponding additive white Gaussian noise.

The limited number of paths in the mm-wave channels imposes a sparse structure in the angular domain which can be used for reducing the number of RF chains at the BS. In the next section this sparsity will be used for designing a reduced rank RF combiner for sparse mm-wave channel estimation.

4.3 Multi-band mm-wave channel estimation

4.3.1 Multi-band Structure of mm-wave channels

In this section we aim to use the sparsity of mm-wave channel in the angular domain to model the received signal as a multi-band signal and propose a channel estimator using a few number of RF chains.

The continuous spatial Fourier transform (CSFT) of $h_k(\hat{s},p)$, namely the angular

channel, can be defined as,

$$\hat{h}_k(f^a, p) = \int_{-\infty}^{\infty} h_k(\hat{s}, p) e^{-j2\pi f^a \hat{s}} d\hat{s} \tag{4.3}$$

where f^a is called the continuous spatial/angular frequency. Considering the channel model defined in (4.1), $\hat{h}_k(f^a, p)$ can be simplified as,

$$\hat{h}_k(f^a, p) = \sum_{l=0}^{L_k-1} \alpha_{l,k} e^{-j2\pi f_s \tau_{l,k} p/P} \delta\left(f^a - \frac{\sin(\theta_{l,k})}{\lambda}\right) \tag{4.4}$$

which indicates that $\hat{h}_k(f^a, p)$ is a sparse signal only being nonzero at $\{f^a = \sin(\theta_{l,k})/\lambda\}_{l=0}^{L_k-1}$. Using the Fourier transform properties, it can be easily verified that limiting $\hat{s}$ to the BS antenna array length, i.e., $\hat{s} \in [0, (N_{BS}-1)d]$, leads the delta functions in (4.4) being replaced with the sinc functions as follows

$$\hat{h}_k(f^a, p) = (N_{BS}-1)d \sum_{l=0}^{L_k-1} \alpha_{l,k} e^{-j2\pi f_s \tau_{l,k} p/P} \text{sinc}\left((f^a - \frac{\sin(\theta_{l,k})}{\lambda})(N_{BS}-1)d\right) \tag{4.5}$$

where $\text{sinc}(f^a) = \sin(\pi f^a)/(\pi f^a)$. The nonzero angular bandwidth imposed by the sinc functions indicates the power leakage from the nonzero angular frequencies of (4.4) to their adjacent frequencies. The smaller the length of the antenna array is, the wider are the sinc functions and the more is the power leakage. This encourages us to model the angular channel $\hat{h}_k(f^a, p)$ and correspondingly the angular received signal $\hat{x}_k(f^a, p)$ as a multi-band signal with at most L_k distinct sub-bands at $\{f^a = \sin(\theta_{l,k})/\lambda\}_{l=0}^{L_k-1}$ and each having a bandwidth of

$$\beta \geq \frac{2}{(N_{BS}-1)d} \tag{4.6}$$

where the lower bound of β is equal to the main lobe width of the sinc function in (4.5). Since, the main lobe of the sinc function contains more that 90% of its total power [87], we approximate β by its lower bound in the rest of this chapter. It should

be also noted that the location of the sub-bands are independent of the sub-carrier index p which means that for each user the channel of all sub-carriers follow the same sparsity structure.

It is clear from (4.5) that the maximum angular bandwidth of $\hat{h}_k(f^a, p)$ is limited to $F = [-\frac{1}{\lambda} - \frac{\beta}{2}, \frac{1}{\lambda} + \frac{\beta}{2}]$ which, based on the Nyquist theorem, implies that the distance between the adjacent antennas should satisfy

$$d \leq \frac{1}{2/\lambda + \beta} = \frac{\lambda}{2} - \frac{\lambda}{N_{BS} - 1} \approx \frac{\lambda}{2} \tag{4.7}$$

where the approximation in (4.7) is based on the fact that for mm-wave MIMO systems λ and N_{BS} are pretty small and big, respectively. Moreover, using $d = \frac{\lambda}{2}$, it can be easily verified that the maximum angular bandwidth can be approximate as $F \approx [-\frac{1}{2d}, \frac{1}{2d}]$.

Ignoring the additive noise effect, Fig. 4.1 (a) shows a schematic diagram of $\hat{x}_k(f^a, p)$. The user index k is dropped in Fig. 4.1 and the rest of this chapter for notation simplicity.

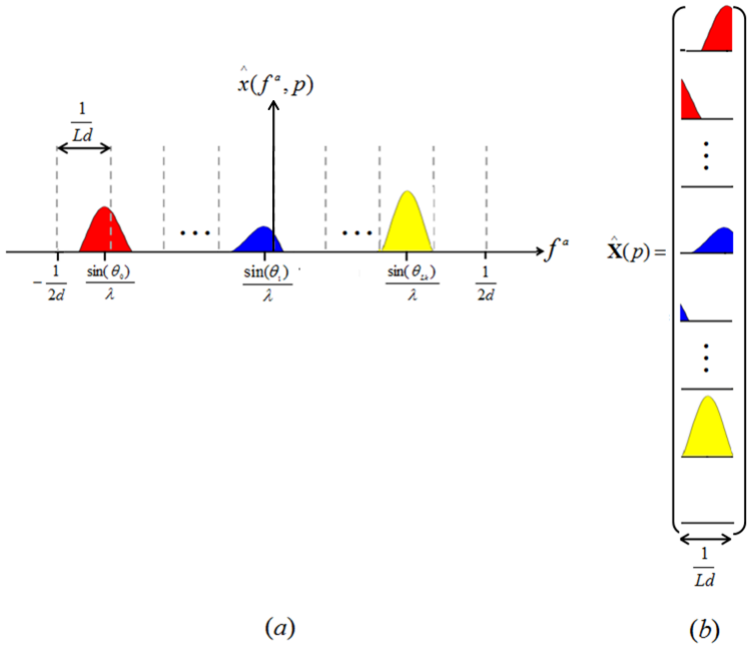

Figure 4.1: (a) Schematic diagram of the spatial spectrum of the received signal at sub-carrier p. (b) Related schematic of $\hat{\mathbf{X}}(p)$ matrix

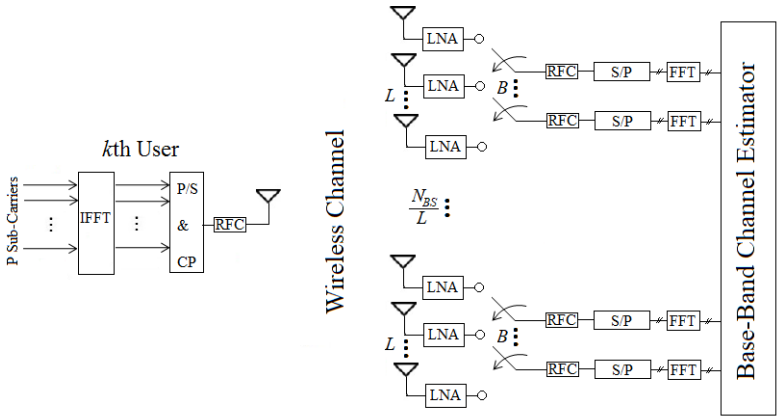

Figure 4.2: Proposed switch-based hybrid architecture

4.3.2 Proposed Channel Estimation Method

Considering the multi-band structure of the channel, we propose a channel estimation scheme which can be implemented using a low power switch-based hybrid architec-

ture as shown in Fig. 4.2. This subsection explains the theory behind this channel estimator and Subsection III-C gives the detailed description of the receiver hybrid architecture. The proposed channel estimator is based on the multi-band spectrum reconstruction scheme proposed in 2009 by Mishali in which a multi-coset sampling pattern is used together with the compressed sensing technique for reconstructing the sparse multi-band signal in lower than Nyquist rate [86].

For multi-coset sampling of the spatial domain received signal, the BS antennas are divided into blocks of length L. Out of the L antennas of the first block, $B \leq L$ antennas are chosen randomly with $b_i \in \{0, 1, \cdots, (L-1)\}$ indicating the index of the ith chosen antenna. Each of these B antennas accompanying with the antennas of the same index in the next blocks make a uniform sub-set of antennas located at Ld distance from each other. The ith sub-sequence of the spatial domain samples obtained at the ith antenna sub-set is defined as [88, 89],

$$x_i[s,p] = \begin{cases} x(sd,p) & s \in \{nL + b_i\}_{n=0}^{N_i-1} \\ 0 & \text{others} \end{cases} \tag{4.8}$$

where depending on b_i, the number of nonzero samples of the ith sub-sequence, N_i, is limited to

$$\lfloor \frac{N_{BS}}{L} \rfloor \leq N_i \leq \lfloor \frac{N_{BS}}{L} \rfloor + 1. \tag{4.9}$$

The following relationship exists between the discrete spatial Fourier transform (DSFT) of the ith sub-sequence, $\hat{x}_i\left(e^{j2\pi f^a d}, p\right)$, and the CSFT of the spatial domain received signal, $\hat{x}(f^a, p)$, over $f^a \in F_0 = [-\frac{1}{2d}, -\frac{1}{2d} + \frac{1}{Ld})$ [90],

$$\begin{aligned} \hat{x}_i\left(e^{j2\pi f^a d}, p\right) &= \sum_{s=-\infty}^{\infty} x_i[s,p] e^{-j2\pi f^a sd} \\ &= \frac{1}{Ld} \sum_{l=0}^{L-1} e^{\frac{j2\pi b_i l}{L}} \hat{x}(f^a + \frac{l}{Ld}, p). \quad for \quad i = 1, ..., B \end{aligned} \tag{4.10}$$

It is clear from (4.10) that $\hat{x}_i\left(e^{j2\pi f^a d}, p\right)$ at each $f^a \in F_0$ contains the effect of $\hat{x}(f^a, p)$ at L equally spaced angular frequencies starting from f^a and with distance $\frac{1}{Ld}$ from each other, i.e., $\left\{f^a + \frac{l}{Ld}\right\}_{l=0}^{L-1}$. So, when f^a changes over F_0, $\hat{x}_i\left(e^{j2\pi f^a d}, p\right)$ will contain the effect of $\hat{x}(f^a, p)$ over its whole bandwidth, i.e., $f^a \in F$, which offers the idea of leveraging the information contained in DSFT of the B sub-sequences over F_0 for estimating $\hat{x}(f^a, p)$ over F. To this end, we can rewrite (4.10) in a matrix-vector form as

$$\hat{\mathbf{y}}(f^a, p) = \mathbf{A}\hat{\mathbf{x}}(f^a, p) \quad for \quad f^a \in F_0 \tag{4.11}$$

where $\hat{\mathbf{y}}(f^a, p)$ contains the DSFT of the B sub-sequences at f^a and $\hat{\mathbf{x}}(f^a, p)$ contains the CSFT of the received signal at L corresponding frequencies as follows,

$$[\hat{\mathbf{y}}(f^a, p)]_i = \hat{x}_i\left(e^{j2\pi f^a d}, p\right) \quad i = 1, 2, \cdots, B \tag{4.12a}$$

$$[\hat{\mathbf{x}}(f^a, p)]_l = \hat{x}(f^a + \frac{l-1}{Ld}, p) \quad l = 1, 2, \cdots, L \tag{4.12b}$$

$$[\mathbf{A}]_{i,l} = \frac{1}{Ld}\exp\left(\frac{j2\pi b_i(l-1)}{L}\right) \quad i = 1, 2, \cdots, B \quad and \quad l = 1, 2, \cdots, L. \tag{4.12c}$$

So, for recovering $\hat{x}(f^a, p)$ over F one can solve (4.11) for estimating $\hat{\mathbf{x}}(f^a, p)$ for each $f^a \in F_0$. We also define $\hat{\mathbf{X}}(p)$ as a matrix containing the $L \times 1$ vectors $\hat{\mathbf{x}}(f^a, p)$ for $f^a \in F_0$ as its columns. Since F_0 is a continuous interval, the number of columns of $\hat{\mathbf{X}}(p)$ tends to infinity. Based on the definition of $\hat{\mathbf{x}}(f^a, p)$ presented in (4.12b), it is clear that the infinite column matrix $\hat{\mathbf{X}}(p)$ is obtained by dividing $\hat{x}(f^a, p)$ into the intervals of length $\frac{1}{Ld}$ and choosing each of the intervals as one of its rows. Fig. 4.1 (b) shows a schematic diagram of the infinite column matrix $\hat{\mathbf{X}}(p)$ for the corresponding angular spectrum presented in Fig. 4.1 (a). It is obvious from Fig. 1(b) that each column of $\hat{\mathbf{X}}(p)$ and equivalently $\hat{\mathbf{x}}(f^a, p)$ for each $f^a \in F_0$ has a limited number of

nonzero entries. So, $\hat{\mathbf{x}}(f^a, p)$ is a sparse vector which can be determined uniquely by finding the sparsest solution of (4.11) if its sparsity level satisfies [91],

$$\|\hat{\mathbf{x}}(f^a, p)\|_0 \leq \frac{\phi(\mathbf{A})}{2}. \tag{4.13}$$

In this equation $\|\hat{\mathbf{x}}(f^a, p)\|_0$ indicates the number of nonzero elements of $\hat{\mathbf{x}}(f^a, p)$, and $\phi(\mathbf{A}) \leq B$ is the Kruskal rank of matrix $\mathbf{A}$ which takes its maximum value when all the columns of $\mathbf{A}$ are linearly independent. The sampling pattern which leads to $\phi(\mathbf{A}) = B$ is called the universal sampling pattern. The multi-coset sampling pattern of (4.8) would be universal if L is chosen as a prime number [92]. Following theorem 3 of [86] the sufficient conditions for satisfying (4.13) is obtained as follows.

Corollary 1 [86]: Assume a multi-band signal with bandwidth of $[-\frac{1}{2d}, \frac{1}{2d}]$ and L_k sub-bands each has a maximum bandwidth of β. If:

1) $L \leq 1/\beta d$

2) $B \geq 2L_k$

3) sampling pattern of (4.8) is universal,

then, for every $f^a \in F_0$, (4.13) is satisfied and (4.11) has a unique L_k-sparse solution.

Based on the above-mentioned conditions, for complete channel estimation, (4.11) should be solved for each $f^a \in F_0$ and each sub-carrier using the CS recovery algorithms which is highly computationally complex due to the continuity of F_0 and high number of sub-carriers. In the following we try to recover the continuous spectrum of the channel by solving a finite dimensional problem, rather than solving the infinite number of linear systems of (4.11), based on the ideas presented in [86] and the same sparse structure of the sub-carriers. The presented formulations differs from those of [86] in that we consider an extra dimension related to sub-carriers in our analysis compared to the narrowband signal considered in [86].

We define a new matrix $\hat{\mathbf{X}}_p$ obtained by cascading the continuous matrices $\hat{\mathbf{X}}(p)$

for $p \in \{1, 2, \cdots, P\}$ as follows,

$$\hat{\mathbf{X}}_p = \begin{bmatrix} \hat{\mathbf{X}}(1) & \hat{\mathbf{X}}(2) & \cdots & \hat{\mathbf{X}}(P) \end{bmatrix} \tag{4.14}$$

since all sub-carriers have the same support set, the place of the nonzero rows of $\hat{\mathbf{X}}_p$ also will be the same as that of $\hat{\mathbf{X}}(p)$ for each $p \in \{1, 2, \cdots, P\}$. Our aim is to find the index set of the nonzero rows of the $\hat{\mathbf{X}}_p$, shown by $\mathcal{S}$, instead of finding the locations of nonzero elements of $\hat{\mathbf{x}}(f^a, p)$ for each $f^a \in F_0$ and each $p \in \{1, 2, \cdots, P\}$. Once $\mathcal{S}$ is determined, $\hat{\mathbf{x}}(f^a, p)$ can be reconstructed for every $f^a \in F_0$ at all sub-carriers simultaneously through a simple matrix inversion problem, by rewriting (4.11) as follows,

$$\hat{\mathbf{Y}}(f^a) = \mathbf{A}_{\mathcal{S}} \hat{\mathbf{X}}^{\mathcal{S}}(f^a) \quad for \quad f^a \in F_0 \tag{4.15}$$

where the $P \times |\mathcal{S}|$ matrix $\mathbf{A}_{\mathcal{S}}$ is obtained by column restriction of $\mathbf{A}$ to $\mathcal{S}$ and the $B \times P$ matrix $\hat{\mathbf{Y}}(f^a)$ contains $\hat{\mathbf{y}}(f^a, p)$ defined in (4.12a) as its pth column. $\hat{\mathbf{X}}^{\mathcal{S}}(f^a)$ is a $|\mathcal{S}| \times P$ matrix with $\hat{\mathbf{x}}(f^a, p)$ defined in (4.12b) as its pth column and row restriction to $\mathcal{S}$. Since the conditions of corollary 1 implies that $|\mathcal{S}| \leq \phi(\mathbf{A})$, $\mathbf{A}_{\mathcal{S}}$ would be a full column rank matrix and the spectrum can be recovered at nonzero places from (4.15) as follows,

$$\hat{\mathbf{X}}^{\mathcal{S}}(f^a) = \mathbf{A}_{\mathcal{S}}^{\dagger} \hat{\mathbf{Y}}(f^a) \quad for \quad f^a \in F_0 \tag{4.16}$$

where $\mathbf{A}_{\mathcal{S}}^{\dagger}$ is the pseudo inverse of $\mathbf{A}_{\mathcal{S}}$. Once the continuous angular spectrum is recovered using (4.16), a simple peak detection algorithm can be used to extract the AOA and the complex gain of each path and reconstruct the continuous spatial domain channel from (4.1). According to (4.5) and as it is shown in Fig. 4.1(a), $\sin(\theta_{l,k})/\lambda$ is equal to the frequency (location) of the lth peak and $\alpha_{l,k} e^{-j2\pi p f_s \tau_{l,k}/P}$ is obtained from the corresponding peak amplitude divided by $(N_{BS} - 1)d$ for each sub-carrier. .

For determining $\mathcal{S}$, we first develop the following matrix relationship from (4.11) which is the same as (4.15) without any column or row restrictions.

$$\hat{\mathbf{Y}}(f^a) = \mathbf{A}\hat{\mathbf{X}}(f^a) \quad for \quad f^a \in F_0 \tag{4.17}$$

Multiplying both sides of (4.17) in their conjugate transpose and then integrating each side over the F_0 interval leads to the following matrix relationship,

$$\mathbf{Q} = \mathbf{A}\mathbf{Z}_0\mathbf{A}^H \tag{4.18}$$

where

$$\mathbf{Q} = \sum_{p=1}^{P} \left(\int_{f=F_0} \hat{\mathbf{y}}(f^a, p)\hat{\mathbf{y}}^H(f^a, p)df^a \right) \tag{4.19a}$$

$$\mathbf{Z}_0 = \sum_{p=1}^{P} \left(\int_{f=F_0} \hat{\mathbf{x}}(f^a, p)\hat{\mathbf{x}}^H(f^a, p)df^a \right) \tag{4.19b}$$

and using the simple matrix rules it can be easily verified that [93],

$$\mathbf{Z}_0 = \sum_{p=1}^{P} \hat{\mathbf{X}}(p)\hat{\mathbf{X}}(p)^H = \hat{\mathbf{X}}_P\hat{\mathbf{X}}_P^H \tag{4.20}$$

which indicates that the index set of the nonzero rows of $\hat{\mathbf{X}}_p$ is the same as that of $\mathbf{Z}_0$ and $\mathcal{S}$ can be determined by finding the location of nonzero rows of $\mathbf{Z}_0$ in (4.18). Following proposition 2 and 3 of [86], the required conditions for unique recovery of $\mathbf{Z}_0$ through an MMV problem are presented in Corollary 2 and 3.

Corollary 2 [86]: If $\mathbf{Q} \geq 0$ and $\mathbf{A}$ are $B \times B$ and $B \times L$ matrices, respectively and

the $L \times L$ matrix $\mathbf{Z}$ satisfies

$$\mathbf{Q} = \mathbf{A}\mathbf{Z}\mathbf{A}^H \tag{4.21a}$$

$$\mathbf{Z} \geq 0 \tag{4.21b}$$

$$|\mathcal{S}_{\mathbf{Z}}| \leq \phi(\mathbf{A}) \tag{4.21c}$$

then, $rank(\mathbf{Z}) = rank(\mathbf{Q})$. Moreover, there can be only a unique matrix $\mathbf{Z}$ satisfying (4.21a) and (4.21b) and

$$|\mathcal{S}_{\mathbf{Z}}| \leq \phi(\mathbf{A})/2 \tag{4.22}$$

with $|\mathcal{S}_{\mathbf{Z}}|$ indicating the number of nonzero rows of $\mathbf{Z}$.

Corollary 3 [86]: Suppose $\mathbf{Z}_0$ satisfies (4.21a), (4.21b) and (4.22) and $\mathbf{Q}$ can be decomposed as $\mathbf{Q} = \mathbf{M}\mathbf{M}^H$ such that $\mathbf{M}$ is a $B \times r$ matrix with r orthogonal columns and r is the rank of $\mathbf{Q}$. Then $\mathbf{D}_0$ is the unique sparsest solution of

$$\mathbf{M} = \mathbf{A}\mathbf{D} \tag{4.23}$$

and $\mathbf{Z}_0 = \mathbf{D}_0\mathbf{D}_0^H$.

So, based on corollary 3, the index set of nonzero rows of $\mathbf{Z}_0$ and $\mathbf{D}_0$ are the same. Therefore, for obtaining $\mathcal{S}$, we can decompose $\mathbf{Q}$ using singular value decomposition to obtain $\mathbf{M}$ as [93],

$$\mathbf{M} = \mathbf{U}\Sigma^{1/2} \tag{4.24}$$

where the $r \times r$ diagonal matrix Σ contains the nonzero singular values of $\mathbf{Q}$ and the $B \times r$ matrix $\mathbf{U}$ contains its corresponding eigenvectors. Then, MMV recovering algorithms can be used for finding the sparsest solution of (4.23), $\mathbf{D}_0$, and correspondingly the index set $\mathcal{S}$.

For computing $\mathbf{Q}$ we can skip the continuous integration calculation in (4.19a) and obtain the elements of $\mathbf{Q}$ using the spatial samples of sub-sequences based on the following relationship,

$$[\mathbf{Q}]_{i1,i2} = \sum_{p=1}^{P} \int_{-\infty}^{+\infty} \left(\hat{x}_{i1}\left(e^{j2\pi f^a d}, p\right) H_{LPS}(f^a)\right) \left(\hat{x}_{i2}\left(e^{j2\pi f^a d}, p\right) H_{LPS}(f^a)\right)^* df^a \quad (4.25)$$
$$= \sum_{p=1}^{P} \sum_{s=-\infty}^{+\infty} \left(x_{i1}[s,p] \circledast h_{LPS}[s]\right) \left(x_{i2}[s,p] \circledast h_{LPS}[s]\right)^*$$

where $\circledast$ indicates the convolution operation and H_{LPS} and h_{LPS} are the transfer function and impulse response of a low-pass filter with cut-off frequency of $\frac{1}{Ld}$, respectively. H_{LPS} is applied for changing the limitation of integration (4.19a) to infinity so that the Parseval theorem can be used for deriving (4.25).

It should be also noted that based on the first condition of corollary 1 and considering Fig. 4.1 (b), each sub-band occupies at most two rows of $\hat{\mathbf{X}}_p$ which leads to $|\mathcal{S}| \leq 2L_k$. So, considering the maximum value of $|\mathcal{S}| = 2L_k$ and the universal sampling pattern ($\phi(\mathbf{A}) = B$), it can be derived from (4.22) that

$$B \geq 4L_k \quad (4.26)$$

which indicates the minimum number of subsets required for unique recovery of $\mathbf{D}_0$. The sampling parameter L can be also approximated as

$$4L_k \leq L \leq \frac{N_{BS} - 1}{2} \quad (4.27)$$

where the lower bound is obtained based on $L \geq B$ and (4.26) and the upper bound is determined from the first condition of corollary 1 where the maximum bandwidth β is approximated by its lower bound in (4.6).

Algorithm 2 summarizes the proposed multi-band MMV channel estimation scheme discussed in this section. It is clear from (4.17)-(4.25) that the index set $\mathcal{S}$ is derived

in a continuous frame work and without any discretization. The angular frequency discretization only appears in (4.16) to obtain the angular spectrum with desired resolution of $1/(LdN_f)$ where N_f is the number of discrete frequencies selected in F_0. It is clear that increasing the angular frequency resolution does not impose any restriction on the sparsity level or the sampling requirements and can improve the peak detection at the cost of more computational complexity in the base-band domain. However, $\mathbf{A}_{\mathcal{S}}^{\dagger}$ in (4.16) is frequency independent and can be calculated just once which helps saving computational resources when increasing the frequency resolution.

Algorithm 2 Proposed Channel Estimation

Input: N_{BS}, d, L_k

Step 1: Choose the sampling parameters B, L from (4.26) and (4.27)

Step 2: Use multi-coset sampling pattern of (4.8) and Compute $\mathbf{Q}$ from (4.25)

Step 3: Use SVD of $\mathbf{Q}$ and define $\mathbf{M}$ as (4.24)

Step 4: Solve (4.23) through an MMV algorithm for the sparsest solution $\mathbf{D}_0$

Step 5: : Define $\mathcal{S}$ as the index set of nonzero rows of $\mathbf{D}_0$ and use (4.16) to recover the angular spectrum

Step 6: Use a peak detection algorithm to extract the AOA and the complex gain of each path based on (4.5).

4.3.3 Hybrid Receiver Design

The proposed channel estimator can be implemented using a hybrid architecture which is known as the switching network architecture [94] and is shown in Fig. 4.2. The RF combiner contains a network of low power switches which are used for antenna sub-set selection based on the multi-coset sampling pattern of (4.8). The number of required switches, N_s, depends on the total number of selected antennas (spatial domain samples) which is controlled by the sampling parameters B and L. The minimum possible number of switches, N_s^{min}, is obtained when B and L have their minimum and maximum possible values minimizing the number of sub-sequences and

the number of samples in each sub-sequence, respectively. Using (4.26) and (4.27) the lower bound and upper bound of N_s^{min} can be defined as

$$8L_k \leq N_s^{min} \leq 8L_k + (N_{BS})\text{mod}(L) \tag{4.28}$$

where the second term in the upper bound is for the case of N_{BS} not being a multiple of L and the possible choice of the first $(N_{BS})\text{mod}(L)$ antennas of each block in the multi-coset sampling pattern. The signals of the selected antennas are then down converted using $N_{RF} = N_s$ RF chains and passed through the serial to parallel and FFT blocks to estimate the channel of each sub-carrier using the base-band channel estimator proposed in Algorithm 2.

Base on the analysis presented in [94] and [95], the proposed hybrid deign is optimum in terms of RF power consumption compared to the other possible RF architectures which may use phase shifter and/or switches with or without analog combining. The RF power consumed by the proposed hybrid combining architecture can be calculated as [94],

$$P = N_{RF}(P_{LNA} + P_{SW}) + N_{RF}(P_{RFC} + P_{ADC}) \tag{4.29}$$

where P_{LNA}, P_{SW}, P_{RFC} and P_{ADC} indicate the power consumed by a single low noise amplifier (LNA), switch, RF chain (RFC) and analog to digital converter, respectively.

4.4 Simulation Results

In this section we present the simulation results for evaluating the performance of the proposed MB-MMV mmWave channel estimator for different system parameters. The simulation parameters are chosen as follows or will be indicated otherwise. For the multi-path channel model of (4.1), we consider Rician fading with $K_{factor} = 20$ dB and the complex path gains $\alpha_{l,k}$ following mutually independent zero-mean complex Gaussian distribution and $\theta_{l,k}$ being uniformly distributed over $[0, 2\pi]$. The carrier

frequency $f_c = 30$ GHz, the sampling frequency $f_s = 0.25$ GHz, the maximum delay spread $\tau_{max} = 100$ ns, $L_{CP} = \tau_{max} f_s = 25$, $P = 32$, $K_u = 4$, $L_k = 4$, $N_{BS} = 128$ and $d = \lambda/2$ [81]. For channel training, one OFDM symbol with $P = 32$ pilot sub-carriers is sent from each user while other users are silent leading to the total training duration of K_u times the OFDM symbol duration and the total pilot load of $K_u P$ sub-carriers. For solving the MMV problem in Step 4 of algorithm 1, we use the regularized M-FOCUSS algorithm which finds the sparse solution of (4.23) by minimizing the following cost function via an iterative algorithm [96],

$$C(\mathbf{D}) = \|\mathbf{AD} - \mathbf{M}\|_F^2 + \gamma J^{\rho,2}(\mathbf{D}) \tag{4.30}$$

Where $\|.\|_F^2$ is the Frobenius norm controlling the quality of fit in the presence of additive noise, and $J^{\rho,2}$ is the diversity measure, controlling the sparsity of the solution which is defined as,

$$J^{\rho,2}(\mathbf{D}) = \sum_{l=1}^{L} \left(\sum_{k=1}^{r} |[\mathbf{D}]_{l,k}|^2 \right)^{\rho/2} \tag{4.31}$$

in which ρ is chosen in the $[0, 1]$ interval guaranteeing the sparsity of the answer and the value of γ determines whether the emphasis is on the sparsity or the quality of fit. More details can be found in [96].

To use the minimum possible number of switches N_s^{min} (correspondingly the minimum possible number of RF chains N_{RF}^{min}), the sampling parameters are chosen as $B = 16$ and $L = 61$ based on (4.26) and (4.27) which according to (4.28) result in $32 \leq N_s^{min}(N_{RF}^{min}) \leq 38$. The number of discrete frequencis in F_0 is set to be $N_f = 40$ leading to the angular frequency resolution of $1/(N_f L d) \approx 0.08$. Fig. 4.3 presents the normalized mean square error (NMSE) of the proposed MB-MMV channel estimator versus SNR obtained from averaging 1000 channel realizations with the average number of used RF chains/switches equals to $N_{RF}^{avg} = N_s^{avg} = \lceil 33.5737 \rceil = 34$. To evaluate the results and using the same pilot pattern, we also adopt the distributed grid match-

ing pursuit (DGMP) algorithm proposed recently in [81] for sparse frequency selective fading channel estimation at mmWave frequencies. The DGMP algorithm considers an adaptive dictionary selection scheme starting with the coarse angular resolution of $1/(N_{BS}d)$ and followed by $J = 19$ times local angular resolution increase leading to the final angular resolution of $1/(N_{BS}Jd) \approx 0.08$ which is the same as the proposed scheme. The DGMP algorithm uses a random CS-based hybrid architecture in which random phase matrices are considered for RF and base-band combiner design. In the DGMP algorithm the number of RF chains equals the combiner size which is chosen as $N_{RF} = 34$ and for each user the dominant path is estimated iteratively. It is clear from Fig. 4.3 that for very low SNRs the DGMP algorithm outperforms the proposed MB-MMV algorithm since for each user it only estimates the LOS while the proposed scheme considers the estimation of all paths. As the K_{factor} is large the NLOS paths would have very small power compared to the LOS and are more probable to be estimated wrongly at very low SNRs which can lead to bigger NMSE for the proposed scheme compared to neglecting the effect of the NLOS paths which is considered in DGMP. As the SNR increases, the performance of the proposed scheme gets better than the DGMP algorithm. In Fig. 4.3, we also present the simulation results for the modified-DGMP algorithm in which the same iterative algorithm as the DGMP algorithm is applied for estimating the NLOS paths as well. While at higher SNRs the performance of the modified-DGMP is better than the DGMP and approaches that of the proposed MB-MMV scheme, it degrades in lower SNRs indicating the weakness of the DGMP algorithm for estimating the NLOS paths at lower SNRs.

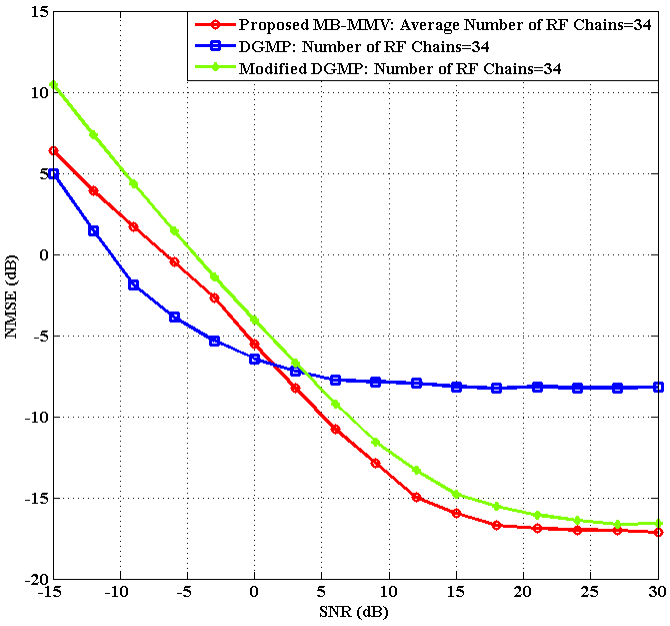

Figure 4.3: Comparison of the NMSE at different SNRs for different channel estimators

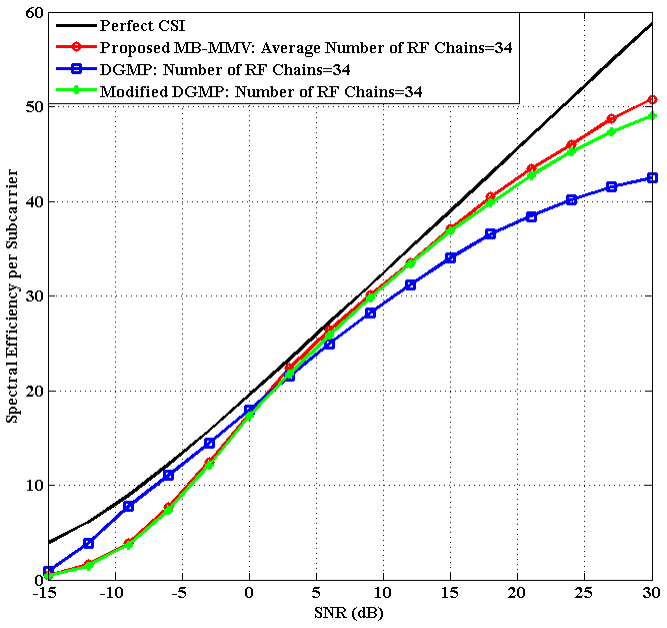

Figure 4.4: Downlink spectral efficiency comparison at different SNRs using the channel information from different estimators

Using the hybrid precoding scheme proposed in [97], Fig. 4.4 evaluates the downlink spectral efficiency performance of the MB-MMV channel estimator versus SNR

for the chosen parameters of Fig. 4.3. The pilot SNR for channel estimation is set to be the same as the SNR for spectral efficiency calculation and the case of perfect channel state information (CSI) at the BS, the DGMP and modified-DGMP algorithms are also presented for comparison. It is clear from Fig. 4.4 that the performance of both the proposed MB-MMV and the modified-DGMP algorithm are close to that of perfect CSI specially for low to moderate SNRs. Moreover, the results are consistent with Fig. 4.3 indicating the better performance of the proposed scheme compared to the DGMP algorithm for SNR > 0 dB.

In Fig. 4.5 and Fig. 4.6 the performance of different channel estimators are evaluated for different number of RF chains and different SNRs. The minimum required number of RF chains for achieving the floor NMSE/ceiling spectral efficiency is smaller for the DGMP and modified-DGMP algorithms compared to the proposed MB-MMV approach; however, the performance of the proposed scheme is better than the DGMP and modified-DGMP algorithms at least for SNR > 0 dB and the number of RF chains satisfying the minimum sampling requirements according to (4.28). For example, at SNR $= 30$ dB and for 34 RF chains, the proposed MB-MMV scheme outperforms the DGMP and modified-DGMP in terms of the NMSE by 9 dB and 0.7 dB and in terms of spectral efficiency by 7 bps/Hz and 1.5 bps/Hz, respectively.

Fig. 4.7 and Fig. 4.8 also compare the results at SNR=15 dB for different K_{factor}s and different number of RF chains. It is clear that the performance of all estimators degrades as the K_{factor} decreases. Moreover, for different K_{factor}s the performance of the MMV-MB algorithm is better than the DGMP and modified-DGMP algorithms for the number of RF chains set to be sufficiently high.

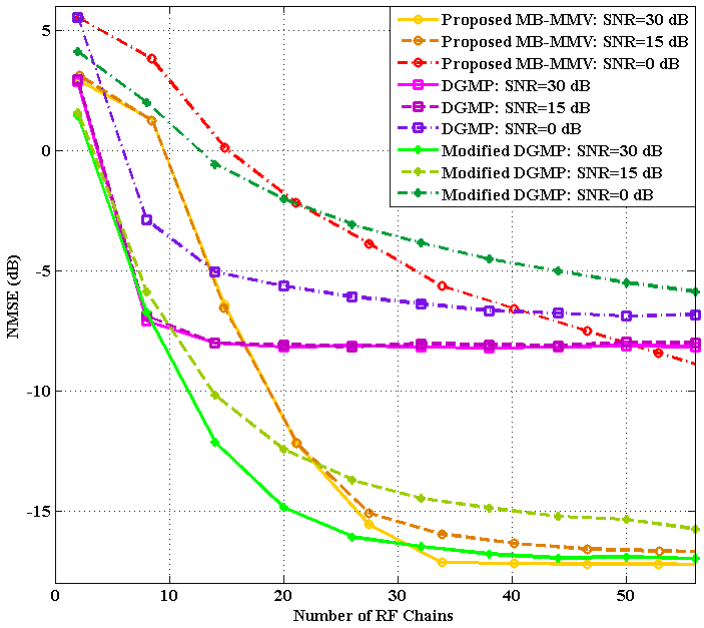

Figure 4.5: Comparison of the NMSE for different channel estimators using different number of RF chains and at different SNRs

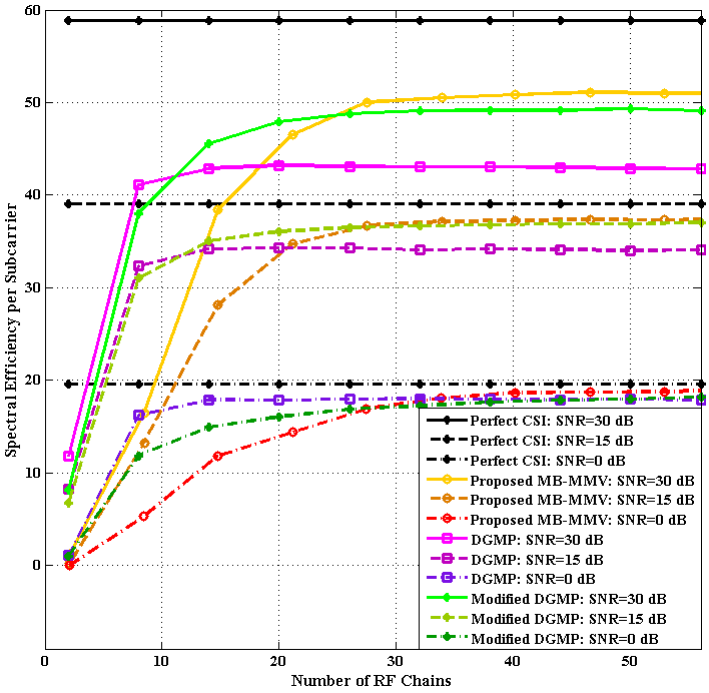

Figure 4.6: Downlink spectral efficiency comparison of different channel estimators using different number of RF chains and at different SNRs

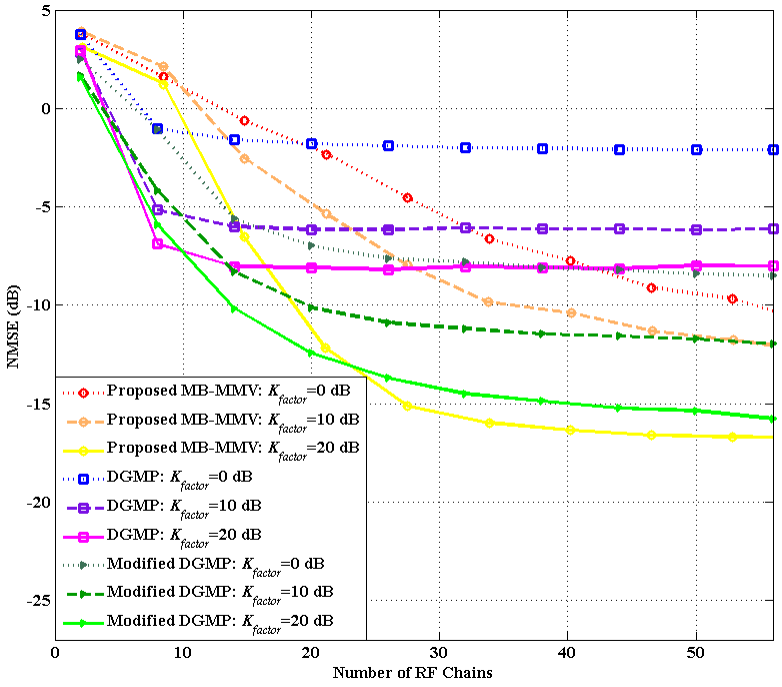

Figure 4.7: Comparison of the NMSE for different channel estimators at SNR=15 dB using different number of RF chains and for different K_{factor}s

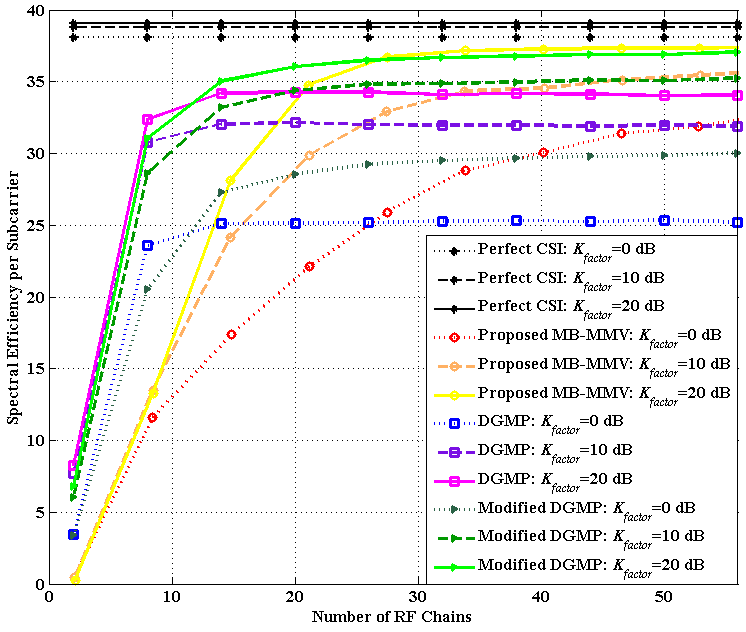

Figure 4.8: Downlink spectral efficiency comparison of different channel estimators at SNR=15 dB using different number of RF chains and for different K_{factor}s

From the RF power consumption point of view, as in the DGMP algorithm a

random phase matrix is considered as the combiner matrix, the RF circuit can be implemented using a phase shifting network and based on the analysis presented in [94] the amount of RF power consumption for the DGMP/modified-DGMP algorithm can be calculated as,

$$P = N_{BS}(N_{RF}+1)P_{LNA} + N_{BS}N_{RF}P_{PS} + N_{RF}(P_{RFC}+P_{ADC}) \quad (4.32)$$

where P_{PS} is the power consumed by a single phase shifter. Considering $P_{ref} = 20$ mW and $P_{LNA} = P_{ref}, P_{ADC} = 10P_{ref}, P_{RFC} = 2P_{ref}, P_{PS} = 1.5P_{ref}, P_{SW} = 0.25P_{ref}$, Fig. 4.9 compares the amount of RF power consumption for the MB-MMV, DGMP and modified-DGMP algorithms for different number of RF chains. The curves in Fig. 4.9 show that the proposed MB-MMV algorithm achieves an order of magnitude power saving than DGMP and modified-DGMP algorithms.

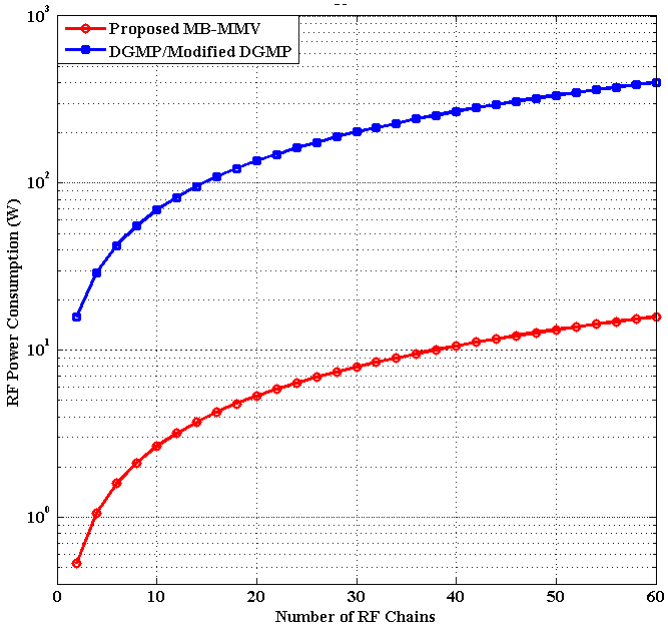

Figure 4.9: RF power consumption for different number of RF chains

For comparing the computational load of the proposed MB-MMV channel estimator with the DGMP and modified-DGMP algorithms, the computational complexity is computed in terms of the number of complex multiplications for each of the al-

gorithms. Considering N_{MMV} as the average number of iterations required by the MMV algorithm for converging to the unique sparsest solution of (4.23), the total computational complexity of the proposed MB-MMV approach, for recovering the angular spectrum of one user, can be approximated as $C_{MB-MMV} \approx N_{MMV}(B^3 + B^2L + B(2L^2 + 2LL_k) + 6LL_k) + B^3 + B^2 + B(3(\lfloor \frac{N_{BS}}{L} \rfloor + 1)^2 + 2N_f Lk)P + 16LL_k^2 + 8L_k^3$. Similarly, the computational complexity of the modified-DGMP algorithm per each user is calculated as $C_{M-DGMP} \approx N_{M-DGMP}N_{RF}PL_kK_u(N_{BS}^2 + (2J+1)N_{BS} + 4J) + N_{M-DGMP}PL_k(N_{BS} + 2J) + PK_uN_{BS}(K_uN_{RF} + 1)$ with N_{M-DGMP} being the average number of required iterations for estimating the AOA of each path in the modified-DGMP algorithm. The complexity of the DGMP algorithm can be approximated from C_{M-DGMP} by replacing L_k by one and N_{M-DGMP} by the number of iterations required for estimating the AOA of the LOS component of each user. Fig. 4.10 compares the computational complexity of different algorithms for different number of RF chains. The number of iterations for each algorithm and each choice of number of RF chains is obtained by averaging over 1000 channel realizations and different ranges of SNRs. It is clear that the proposed MB-MMV channel estimator has orders of magnitude lower computational complexity than the DGMP and modified-DGMP algorithms. The slight complexity reduction of the proposed MB-MMV algorithm at high number of RF chains is the result of better convergence rate of the MMV algorithm when the number of RF chains increases beyond the minimum requirement.

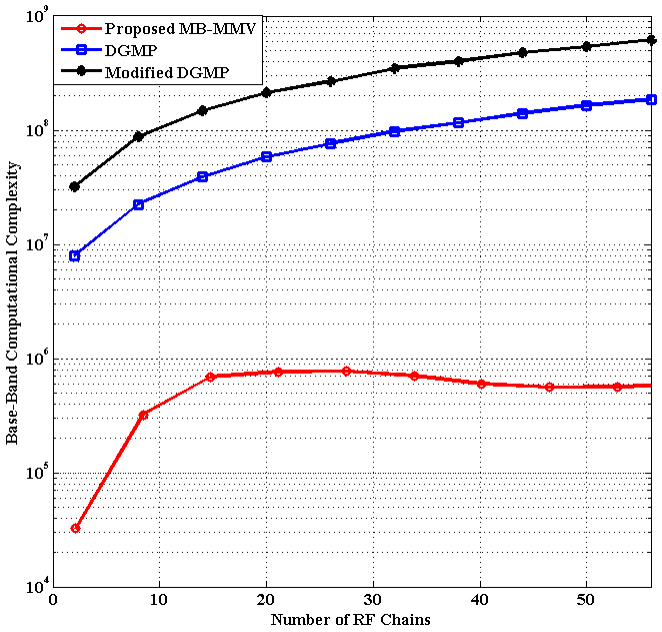

Figure 4.10: Base-band computational complexity for different number of RF chains

4.5 Conclusion

In this chapter, we have proposed a CS-based channel estimator for the mmWave MIMO-OFDM system with a switch-based low power hybrid combiner. A multi-band structure is considered for the continuous angular channel and the angular support is recovered without the need for any discretization by solving a finite dimensional MMV problem in which the same sparsity structure of all sub-carriers is considered to further reduce the computational complexity of the problem. The proposed MB-MMV channel estimator combats the inherent limited angular resolution and power leakage problem of the existing CS based channel estimators which treat the channel in a discrete framework with quantized angle grids. The minimum number of required RF chains for unique recovery of the channel has been determined based on the number of channel's multipath components and the simulation results confirms the effectiveness of the proposed scheme in terms of the estimation accuracy, RF power consumption and the base-band computational complexity.

Chapter 5

Conclusion and Future Research Issues

5.1 Conclusion

In this dissertation, we have investigated the low dimensional channel estimation and channel prediction for fast time varying channels and the hybrid channel estimation for mm-wave communication systems. The conclusions are drawn as follows:

- **Reduced Rank MIMO-OFDM Channel Estimation for High Speed Railway Communication using 4D Generalized DPS Sequences**

  Considering a regular shape geometry-based stochastic channel model, we have exploited the correlation of the MIMO-OFDM HSR channel in time, frequency and spatial domain for representing it based on a 4D basis expansion model which is spanned by limited number of time-concentrated and band limited GDPS sequences. Using the low-dimensional basis expansion channel model, the high dimensional channel estimation problem is converted to the estimation of limited number of basis coefficients which reduces the required pilot overhead. A reduced rank LMMSE estimator has been derived for estimating the basis coefficients without requiring any information about the channel's correlation matrix. The proposed

channel estimator has better performance than the conventional interpolation based LS channel estimation scheme and has lower complexity compared to a full rank LMMSE estimator. The proposed channel estimator has also robust performance for different delay and Doppler spreads based on the simulation results obtained for the train cutting scenario and the non-stationary RS-GBSM propagation channel model. Moreover, it has been shown that for the same pilot overhead, the bigger AOD spread and transmitter antenna array size result in degraded performance of the proposed channel estimator while increasing the AOA spread and the receiver antenna array size can improve the estimation error due to using more basis functions for spanning the spatial domain channel at the receiver side.

- **MIMO Channel Prediction for Fast Time-Variant Flat Fading Channels based on DPS Sequences**

  We have developed a new sub-frame wise channel tracking scheme for the fast time variant channels which considers the transmitted frame to be segmented into several sub-frames and exploits the variation of the channel inside each sub-frame using a low-dimensional DPS basis expansion model and applies a Q-order AR model for tracking the variation of the basis coefficients through the whole frame. The error contribution from the DPS basis expansion modelling of the channel coefficients and the AR tracking of the basis coefficients have been investigated and it is shown that for the stationary channels the DPS reconstruction error is independent of the subframe index. The simulation results, presented for the Jakes's fading channel model, demonstrate the smaller error contribution from the DPS modelling of the channel coefficients compared to the AR prediction error of the basis coefficients. Moreover, it has been shown that the less dominant basis have smaller AR prediction error since they have less contribution in channel modelling. An algorithm for obtaining the optimal sub-frame length, the optimal number of basis and the optimal order of the AR model has also been proposed through minimizing the prediction error of the whole frame. As it is expected, the simulation results have

shown that by increasing the maximum normalized Doppler frequency the optimal subframe length decreases and more basis are required per each subframe. Finally, the relative amount of feedback load reduction which can be achieved by the application of the proposed channel tracking scheme for the reduced feedback load and feedback delay precoder design in time-varying systems has been calculated for different MIMO sizes. The simulation results also validate the better performance of the proposed channel prediction scheme compared to the previous minimum energy DPS based channel predictor for all ranges of Doppler frequencies and the out-performance of the proposed channel predictor compared to the conventional AR tracking scheme for low to moderate Doppler frequencies and almost the same performance as it for high Doppler frequencies but with lower amount of computational complexity.

- **Hybrid mm-Wave MIMO-OFDM Channel Estimation Based on the Multi-Band Sparse Structure of Channel**

  Considering the sparse structure of the mm-wave channel in the angular domain, we have developed a new power efficient channel estimation scheme for the mm-wave MIMO-OFDM systems which is implemented using a hybrid architecture. The continuous angular channel has been modelled as a sparse multi-band signal with the number of sub-bands being equal to the number of multi-path components and the bandwidth of each sub-band being proportional to the amount of power leakage caused by the limited antenna array length. A multi-coset sampling pattern has been used for antenna sub-set selection and the sampling parameters have been derived based on the required conditions for the unique recovery of the continuous angular channel from the limited number of spatial domain samples. The sparse channel recovery has been formulated within the CS framework by exploiting the same sparsity structure of all sub-carriers and applying the MMV recovery techniques. A hybrid architecture has been presented for implementing the proposed channel estimator using low power switches and the minimum number of required

RF chains has been obtained based on the chosen sampling parameters. Simulation results have shown that for the number of RF chains satisfying its minimum requirement, the proposed channel estimation scheme offers better performance both in terms of NMSE and the spectral efficiency in comparison to the DGMP and modified-DGMP algorithms at least for SNR $\geq$ 0 dB. For the case of non-sufficient number of RF chains the DGMP and modified DGMP may have better performance than the proposed scheme at the cost of more RF power consumption.

5.2 Future Research Issues

There are several open issues for further research related to the topics in the dissertation.

- The narrowband MIMO precoding techniques proposed in [98, 34, 35] can be extended to MIMO-OFDM by treating the OFDM sub-carriers as a set of parallel narrowband MIMO channels [99]. However, applying the narrowband precoding techniques directly to MIMO-OFDM systems will result in increased data rate in the feedback channel, and the system will become prohibitively costly as the number of subcarriers increases. This has motivated further research to investigate low-rate feedback schemes for MIMO-OFDM systems. Vector quantization and smart interpolation has been proposed, for example in [99, 100], where the receiver sends back only the precoder matrices of a subset of the subcarriers. At the transmitter, the precoders for all other subcarriers are computed using smart interpolation. Clustering based limited feedback techniques were proposed in [101] and [102], where the subcarriers are divided into clusters and one precoder matrix is used for each cluster. A reduced feedback algorithm based on the fact that highly correlated channels have highly correlated feedback values is proposed in [103]. However, these existing methods require sophisticated quantization schemes to minimize information loss. QR decomposition (QRD)-based precoded MIMO-OFDM systems with reduced feedback rates are also proposed in [104] to convert

the MIMO-OFDM channel into layered subchannels and employ the same precoder for all carriers. Hence, as a part of our future work, we could study the statistical properties of the eigen-vectors of random matrices for exploiting the correlation between the eigen-vectors of the channel matrix at different sub-carriers and propose a reduced feedback rate precoder for MIMO-OFDM system. To our best knowledge none of the previous works on MIMO-OFDM precoder design has studied the relationship between the correlation function of the channel coefficients and the correlation function of the eigen-vectors of the channel matrix.

- As discussed in Chapter 3, channel prediction allows for proper tracking of the precoder matrix in time-variant channels. Recently, the channel prediction has been extended to MIMO-OFDM cases. A simplified adaptive channel prediction scheme is proposed in [105], which assumes a WSSUS Rayleigh fading channel for each antenna pair with no spatial correlation among the antennas. Due to the uncorrelated scattering property, different channel taps are independent and only temporal correlation is used for predicting each tap in time domain. Similarly, the prediction methods in [106] and [107] treat every subcarrier of MIMO-OFDM as a narrowband SISO channel, which only consider the temporal correlation for predicting flat-fading channels in frequency domain. These approaches do not exploit the spatial correlation which exists in reality. For example, insufficient spacing between antennas in deployment may bring in inevitable spatial correlation [108]. The spatial correlation can be utilized to improve the performance of channel prediction as indicated in [109]. More recently, [48] developed a MIMO-OFDM prediction framework with improved performance which exploits both the temporal and spatial correlations. The MIMO-OFDM prediction schemes proposed in [105, 106, 107, 108, 109, 110] are based on AR model for which the complexity increases if signals from other antennas are used to improve the channel prediction. We could extend the proposed low complexity DPS-AR channel predictor to the MIMO-OFDM case through using multi-dimensional DPS basis for exploiting

the time, frequency and spatial correlations and improving the channel prediction performance. Morover, we could propose a reduced rank precoder predictor that directly predicts the precoder matrix based on the statistical properties of the eigen-vectors of the channel matrix.

- The proposed mm-wave channel estimator in Chapter 4, assumes single-antenna users. However, the deployment of multi-antennas per device is highly realistic particularly for systems operating at mm-wave frequencies due to the small size of antennas. Applying multi antennas per each user can improve the channel estimation performance specially if proper precoding scheme is used at each user. Similar to the combiner design, some of the previous work consider the hybrid precoder design by exploiting the sparsity of the mm-wave channel and applying random phase matrices for the implementation of the RF precoder matrix [81], [72]. The high RF power consumption of the phase shifters which are required for implementing the random phase matrices motivates the switch based hybrid precoder design. Therefore, we could exploit the multi-band structure of the angular mm-wave channel for proposing a low power hybrid precoder scheme.

Bibliography

[1] A. Ghazal, C. X. Wang, B. Ali, and D. Yuan, "A nonstationary wideband MIMO channel model for high-mobility intelligent transportation systems," *IEEE Transactions on Intelligent Transportation Systems*, vol. 16, no. 2, pp. 885–897, Apr. 2015.

[2] T. Zemen, C. F. Mecklenbruker, B. H. Fleury, and F. Kaltenberger, "Minimum-energy band-limited predictor with dynamic subspace selection for time-variant flat-fading channels," *IEEE Transactions on Signal Processing*, vol. 55, no. 9, pp. 4534–4548, Sep. 2007.

[3] B. Chen and Z. Zhong, "Geometry-based stochastic modeling for MIMO channel in high-speed mobile scenario," *International Journal of Antennas and Propagation*, vol. 2012, pp. 1–6, 2012.

[4] B. Ali, X. Cheng, T. Kurner, and Z. Zhong, "Challenges toward wireless communications for high speed railway," *IEEE Transactions on Intelligent Transportation Systems*, vol. 15, pp. 2143–2158, Oct. 2014.

[5] *LTE/SAE -The Future Railway Mobile Radio System? Long-Term Visions on Railway Mobile Radio Technologies*, UIC Draft, Rev. 0.4, 2009.

[6] G. Tingting and S. Bin, "A high-speed railway mobile communication system based on LTE," in *Proc. IEEE International Conference On Electronics and Information Engineering (MEMS)*, Kyoto, Japan, Aug. 2010, pp. 414–417.

[7] R. S. He, Z. D. Zhong, B. Ai, J. Ding, , and Y. Yang, "Propagation measurements and analysis of fading behavior for high speed rail cutting scenarios," in *Proc. IEEE Globecom*, Anaheim, CA, Dec. 3–7, 2012, pp. 5015–5020.

[8] L. Liu *et al.*, "Position-based modeling for wireless channel on highspeed railway under a viaduct at 2.35 GHz," *IEEE Journal on Selected Areas in Communications*, vol. 30, no. 4, pp. 834–845, May 2012.

[9] K. Guan, Z. Zhong, T. Kurner, and B. Ali, "Propagation measurements and modeling of crossing bridges on high-speed railway at 930 MHz," *IEEE Transactions on Vehicular Technology*, vol. 63, pp. 502–517, Feb. 2014.

[10] J. Qiu, C. Tao, L. Liu, and Z. Tan, "Broadband channel measurement for the high-speed railway based on WCDMA," in *Proc. IEEE 75th Vehicular Technology Conference (VTC Spring)*, Yokohama, Japan, May 2012, pp. 1–5.

[11] P. Hoeher, S. Kaiser, and P. Robertson, "Two-dimensional pilot symbol-aided channel estimation by wiener filtering," in *Proc. IEEE International Conference on Acoustics Speech and Signal Processing (ICASSP-97)*, Munich, Germany, Apr. 1997, pp. 1845–1848.

[12] G. Auer, "3D MIMO-OFDM channel estimation," *IEEE Transactions on Communications*, vol. 60, no. 4, pp. 972–985, 2012.

[13] B. Yang, K. B. Letaief, R. S. Cheng, and Z. Cao, "Channel estimation for OFDM transmission in multipath fading channels based on parametric channel modeling," *IEEE Transactions on Communications*, vol. 49, no. 3, pp. 467–479, Mar. 2001.

[14] T. Zemen and C. Mecklenbrauker, "Time-variant channel estimation using discrete prolate spheroidal sequences," *IEEE Transactions on Signal Processing*, vol. 53, pp. 3597–3607, Sep. 2005.

[15] O. Edfors, M. Sandell, J. J. van de Beek, S. K. Wilson, and P. O. Borjesson, "OFDM channel estimation by singular value decomposition," *IEEE Transactions on Communications*, vol. 46, no. 7, pp. 931–939, Jul. 1998.

[16] J. Du and Y. Li, "D-blast OFDM with channel estimation," *EURASIP Journal on Applied Signal Processing*, vol. 5, pp. 605–612, May 2004.

[17] P. S. Rossi and R. Muller, "Slepian-based two-dimensional estimation of time-frequency variant MIMO-OFDM channels," *IEEE Signal Processing Letters*, vol. 15, pp. 21–24, Jul. 2008.

[18] T. Zemen, L. Bernado, N. Czink, and A. F. Molisch, "Iterative time-variant channel estimation for 802.11p using generalized discrete prolate spheroidal sequences," *IEEE Transactions on Vehicular Technology*, vol. 61, pp. 1222–1233, Mar. 2012.

[19] F. Kaltenberger, T. Zemen, and C. W. Uberhuber, "low complexity geometry-based MIMO channel simulation," *EURASIP Journal in Advances in Signal Processing*, vol. 2007, May 2007.

[20] X. Cheng, C. Wang, D. Laurenson, and S. Salous, "An adaptive geometry-based stochastic model for non-isotropic MIMO mobile-to-mobile channels," *IEEE Transactions on Wireless Communications*, vol. 8, no. 9, pp. 4824–4835, Sep. 2009.

[21] E. 3rd Generation Partnership Project, "Evolved universal terrestrial radio access (E-UTRA); base station (BS) radio transmission and reception," ETSI, Technical Specification , no. 136104V11.8.2, 2014.

[22] F. A. Dietrich and W. Utschik, "Pilot-assisted channel estimation based on second-order statistics," *IEEE Transactions on Signal Processing*, vol. 53, no. 3, pp. 1178–1193, Mar. 2005.

[23] D. Slepian, "Prolate spheroidal wave functions, fourier analysis, and uncertainty v: The discrete case," *The Bell System Technical Journal*, vol. 57, no. 5, pp. 1371–1430, 1978.

[24] D. J. Thomson, "Spectrum estimation and harmonic analysis," *Proceedings of the IEEE*, vol. 70, no. 9, pp. 1055–1096, 1982.

[25] B. Chen, Z. Zhong, B. Ai, and D. Michelson, "The application of semi-deterinistic method on high-speed railway cutting scenario," in *Proc. IEEE General Assembly and Scientific Symposium (URSI GASS)*, Beijing, China, Aug. 2014, pp. 1–4.

[26] P. Kysti *et al.*, "WINNER II channel models," IST WINNER II, Munich, Germany, Tech. Rep. D1.1.2 V1.2, Feb. 2008.

[27] T. Zemen, C. F. Mecklenbruker, J.Wehinger, and R. R. Mller, "Iterative joint time-variant channel estimation and multi-user detection for MCCDMA," *IEEE Transactions on Wireless Communications*, vol. 5, no. 6, pp. 1469–1478, Jun. 2006.

[28] J. Lu, G. Zhu, and C. Briso-Rodriguez, "Fading characteristics in the railway terrain cuttings," in *Proc. IEEE Vehicular Technology Conference (VTC Spring 11)*, Yokohama, Japan, May 2011, pp. 1–5.

[29] C. Dumard and T. Zemen, "Low-complexity MIMO multiuser receiver: A joint antenna detection scheme for time-varying channels," *IEEE Transactions on Signal Processing*, vol. 56, no. 7, pp. 2931–2940, Jul. 2008.

[30] D. Tse and P. Viswanath, *Fundamentals of Wireless Communication*. New York, NY: Cambridge University Press, 2005, ch. 7.

[31] R. W. Heath, J. S. Sandhu, and A. Paulraj, "Antenna selection for spatial multiplexing systems with linear receivers," *IEEE Communications Letters*, vol. 5, no. 4, pp. 142–144, 2001.

[32] D. A. Gore, R. U. Nabar, and A. Paulraj, "Selection an optimal set of transmit antennas for a low rank matrix channel," in *Proc. IEEE Int. Conf. on Acoustics, Speech, and Signal Processing*, vol. 5, Istanbul, Turkey, Jan. 2000, pp. 2785–2788.

[33] D. J. Love and R. W. Heath, "Limited feedback precoding for spatial multiplexing systems using linear receiver," in *Proc. IEEE MILCOM. Conf.*, vol. 5, Oct. 2003, pp. 627 – 632.

[34] D. J. Love and R. Heath, "Limited feedback unitary precoding for spatial multiplexing systems," *IEEE Transactions on Information Theory*, vol. 51, no. 8, pp. 2967–2976, Aug. 2005.

[35] S. Zhou and B. Li, "BER criterion and codebook construction for finite-rate precoded spatial multiplexing with linear receivers," *IEEE Transactions on Signal Processing*, vol. 54, no. 5, pp. 1653–1665, May 2006.

[36] K. Kobayashi, T. Ohtsuki, and T. Kaneko, "MIMO systems in the presence of feedback delay," in *Proc. IEEE Int. Conf. on Communications*, Istanbul, Turkey, Jun. 2006, pp. 4102–4106.

[37] A. S. Kharwat, "Precoded spatial multiplexing MIMO systems in time-varying fading channel," *Journal of Communication*, vol. 9, no. 2, pp. 118–125, Feb. 2014.

[38] R. O. Adeogun, "Channel prediction for mobile MIMO wireless communication systems," Ph.D. dissertation, Victoria Univ. of Wellington, Wellington, New Zealand, May 2015. [Online]. Available: http://hdl.handle.net/10063/3768

[39] J. Andersen, J. Jensen, S. Jensen, and F. Frederisen, "Prediction of future fading based on past measurements," in *IEEE Vehicular Technology Conference*, Amsterdam, Sep. 1999, pp. 151–155.

[40] J. K. Hwang and J. H. Winters, "Sinusoidal modeling and prediction of fast fading processes," in *Proc. IEEE Globecom '98*, vol. 2, Sydney, NSW, Nov. 1998, pp. 892–897.

[41] L. Dong, G. Xu, and H. Ling, "Prediction of fast fading mobile radio channels in wideband communication systems," in *Proc. IEEE Globecom '01*, vol. 6, San Antonio, TX, Nov. 2001, pp. 3287–3291.

[42] R. Vaughan, P. Teal, , and R. Raich, "Short-term mobile channel prediction using discrete scatterer propagation model and subspace signal processing algorithms," in *IEEE Vehicular Technology Conference*, vol. 2, Boston, MA, Sep. 2000, pp. 751–758.

[43] J. Vanderpypen and L. Schumacher, "MIMO channel prediction using ESPRIT based techniques," in *IEEE International Symposium on Personal, Indoor and Mobile Radio Communications*, Athens, Sep. 2007, pp. 1–5.

[44] H. Shirani-Mehr, D. N. Liu, and G. Caire, "Channel state prediction, feedback and scheduling for a multiuser mimoofdm downlink," in *42th Asilomar Conference on Signals, Systems, and Computers*, vol. 6, Pacific Grove, CA, Oct. 2008, pp. 136–140.

[45] A. Du-Hallen, S. Hu, and H. Hallen, "Long-range prediction of fading signals: enabling adaptive transmission for mobile radio channels," *IEEE Signal Processing Magazine*, vol. 17, no. 3, pp. 62–75, May 2000.

[46] S. Prakash and I. McLoughlin, "Predictive transmit antenna selection with maximal ratio combining," in *Proc. IEEE Globecom '09*, vol. 2, Honolulu, HI.

[47] M. Chen, T. Ekman, and M. Viberg, "New approaches for channel prediction based on sinusoidal modeling," *EURASIP Journal on Adv. in Signal Processing*, Jan. 2007.

[48] L. Liu, H. Feng, and T. Yang, "MIMO-OFDM wireless channel prediction by exploiting spatial-temporal correlation," *IEEE Transactions on Wireless Communications*, vol. 13, no. 1, pp. 310–319, Jan. 2014.

[49] H. Hallen, A. Duel-Hallen, T. S. Hu, and M. Lei, "A physical model for wireless channels to provide insights for long range prediction," in *Proc. MILCOM 2002*, vol. 1, Oct. 2002, pp. 627–631.

[50] A. Duel-Hallen, "Fading channel prediction for mobile radio adaptive transmission systems," *Proceedings of the IEEE*, vol. 95, no. 12, pp. 2299–2313, Dec. 2014.

[51] A. Heidari, A. K. Khandani, and D. McAvoy, "Adaptive modelling and long-range prediction of mobile fading channels," *IET Communication*, vol. 4, no. 1, pp. 39–50, Jan. 2010.

[52] K. E. Baddour, C. C. Squires, and T. J. Willink, "Mobile channel prediction with application to transmitter antenna selection for alamouti systems," in *Proc. of 64th IEEE Vehicular Technology Conference (VTC-2006)*, Montreal, QC, Sep. 2006, pp. 1–6.

[53] D. K. Borah and B. T. Hart, "Frequency-selective fading channel estimation with a polynomial time-varying channel model," *IEEE Transactions on Communications*, vol. 47, no. 6, pp. 862–873, Jun. 1999.

[54] K. A. D. Teo, S. Ohno, and T. Hinamoto, "Kalman channel estimation based on oversampled polynomial model for OFDM over doubly-selective channels," in *Proc. IEEE 6th Workshop on Signal Processing Advances in Wireless Communications*, 2005, pp. 116–120.

[55] P. Banelli, R. C. Cannizzaro, and L. Rugini, "Data-aided Kalman tracking for channel estimation in doppler-affected OFDM systems," in *Proc. of IEEE*

international Conference on Acoustics, Speech and Signal Processing - ICASSP '07, Apr. 2007, pp. 133–136.

[56] J. K. Tugnait, S. He, and H. Kim, "Doubly selective channel estimation using exponential basis models and subblock tracking," *IEEE Transactions on Signal Processing*, vol. 58, no. 3, pp. 1275–1289, Mar. 2010.

[57] S. He and J. K. Tugnait, "Decision-directed tracking of doubly-selective channels using exponential basis models," in *Proc. of IEEE international Conference on Communications ICC '08*, May 2008, pp. 5098–5102.

[58] T. Zemen and C. Mecklenbrauker, "Time-variant channel estimation using discrete prolate spheroidal sequences," *IEEE Transactions on Signal Processing*, vol. 53, no. 9, pp. 3597–3607, Sep. 2005.

[59] T. Zemen, L. Bernado, N. Czink, and A. F. Molisch, "Iterative time-variant channel estimation for 802.11p using generalized discrete prolate spheroidal sequences," *IEEE Transactions on Vehicular Technology*, vol. 61, no. 3, pp. 1222–1233, Mar. 2012.

[60] T. Zemen, C. Mecklenbrauker, F. Kaltenberger, and B. Fleury, "Minimum-energy band-limited predictor with dynamic subspace selection for time-variant flat-fading channels," *IEEE Transactions on Signal Processing*, vol. 55, no. 9, pp. 4534–4548, Sep. 2007.

[61] H. T. Nguyen, G. Leus, and N. Khaled, "Precoder and decoder prediction in time-varying MIMO channels," in *Proc. IEEE Workshop on Computational Advances in Multi-Sensor Adaptive Processing (CAMSAP2005)*, 2005, pp. 290–294.

[62] D. Slepian, "Prolate spheroidal wave functions, fourier analysis, and uncertainty v: the discrete case," *The Bell System Technical Journal*, vol. 57, no. 5, pp. 1371–1430, 1978.

[63] S. Semmelrodt and R. Kattenbach, "Investigation of different fading forecast schemes for flat fading radio channels," in *Proc. of 58th IEEE Vehicular Technology Conference (VTC-2003)*, Oct. 2003, pp. 149–153.

[64] S. Kay, *Fundamentals of Statistical Signal Processing: Estimation Theory.* Upper Saddle River, NJ: Prentice Hall, 1993, ch. 12.

[65] Z. Pi and F. Khan, "An introduction to millimeter-wave mobile broadband systems," *IEEE Communications Magazine*, vol. 49, no. 6, pp. 101–107, Jun. 2011.

[66] A. Alkhateeb, O. E. Ayach, G. Leus, and R. W. Heath, "Channel estimation and hybrid precoding for millimeter wave cellular systems," vol. 8, no. 5, pp. 831–846, Oct. 2014.

[67] S. Han, L. Chih-lin, Z. Xu, and C. Rowell, "Large-scale antenna systems with hybrid analog and digital beamforming for millimeter wave 5G," *IEEE Communications Magazine*, vol. 53, no. 1, pp. 186–194, Jan. 2015.

[68] O. E. Ayach, S. Rajagopal, S. Abu-Surra, Z. Pi, and R. W. Heath, "Spatially sparse precoding in millimeter wave MIMO systems," *IEEE Journal on Selected Areas in Communications*, vol. 13, no. 3, pp. 1499–1513, Mar. 2014.

[69] R. W. Heath, N. Gonzalez-Prelcic, S. Rangan, W. Roh, and A. M. Sayeed, "An overview of signal processing techniques for millimeter wave MIMO systems," *IEEE Journal of Selected Topics in Signal Processing*, vol. 10, no. 3, pp. 436–453, Apr. 2016.

[70] D. Ramasamy, S. Venkateswaran, and U. Madhow, "Compressive tracking with 1000-element arrays: A framework for multi-Gbps mm wave cellular downlinks," in *Proc. IEEE Annual Allerton Conference on Communication Control and Computing*, Monticello, IL, USA, Oct. 2012, pp. 690–697.

[71] D. E. Berraki, S. M. D. Armour, and A. R. Nix, "Application of compressive sensing in sparse spatial channel recovery for beamforming in mmwave outdoor systems," in *Proc. IEEE wireless communication network conference*, Istanbul, Turkey, Apr. 2014, pp. 887–892.

[72] A. Alkhateeb, G. Leus, and R. W. Heath, "Compressed-sensing based multi-user millimeter wave systems: How many measurements are needed?" in *Proc. IEEE International Conference on Acoustics, Speech and Signal Processing (ICASSP)*, Brisbane, QLD, Australia, Apr. 2015, pp. 2909–2913.

[73] R. Mendez-Rial, C. Rusu, A. Alkhateeb, and R. W. H. N. Gonzalez-Prelcic, "Channel estimation and hybrid combining for mmwave: Phase shifters or switches?" in *Proc. IEEE Information Theory and Applications*, San Diego, CA, USA, Feb. 2015, pp. 90–97.

[74] J. Brady, N. Behdad, and A. M. Sayeed, "Beamspace MIMO for millimeter-wave communications: System architecture modeling analysis and measurements," *IEEE Transactions on Antennas and Propagation*, vol. 61, no. 7, pp. 3814–3827, Jul. 2013.

[75] A. M. Sayeed, "Deconstructing multi-antenna fading channels," *IEEE Transactions on Signal Processing*, vol. 61, no. 7, pp. 2563–2579, Oct. 2002.

[76] A. M. Sayeed, T. Sivanadyan, K. J. R. Liu, and S. Haykin, "Wireless communication and sensing in multipath environments using multi-antenna transceivers," in *Handbook on Array Processing and Sensor Networks*. Piscataway, NJ, USA: IEEE Press, 2010.

[77] J. Lee, G.-T. Gil, and Y. H. Lee, "Channel estimation via orthogonal matching pursuit for hybrid MIMO systems in millimeter wave communications," *IEEE Transactions on Communications*, vol. 64, no. 6, pp. 2370–2386, Jun. 2016.

[78] J. A. Tropp and A. C. Gilbert, "Signal recovery from random measurements via orthogonal matching pursuit," *IEEE Transactions on Information Theory*, vol. 53, no. 12, pp. 4655–4666, Dec. 2007.

[79] D. L. Donoho, "Compressed sensing," *IEEE Transactions on Information Theory*, vol. 52, no. 4, pp. 1289–1306, Apr. 2006.

[80] J. Lee, G. Gye-Tae, and Y. H. Lee, "Exploiting spatial sparsity for estimating channels of hybrid MIMO systems in millimeter wave communications," in *Proc. IEEE Globecom*, SAustin, TX, USA, Dec. 2014, pp. 3326–3331.

[81] Z. Gao, C. Hu, L. Dai, and Z. Wang, "Channel estimation for millimeter- wave massive MIMO with hybridprecoding over frequency-selective fading channels," *IEEE Communications Letters*, vol. 20, no. 6, pp. 1259 – 1262, Apr. 2016.

[82] A. Alkhateeb, G. Leus, and R. Heath, "Limited feedback hybrid precoding for multi-user millimeter wave systems," *IEEE Transactions on Wireless Communications*, vol. 14, no. 11, pp. 6481–6494, Jul. 2015.

[83] J. Brady, N. Behdad, and A. Sayeed, "Beamspace MIMO for millimeter-wave communications: System architecture, modeling, analysis, and measurements," *IEEE Transactions on Antennas and Propagation*, vol. 61, no. 7, pp. 3814–3827, Mar. 2013.

[84] Y. Zeng, R. Zhang, and Z. N. Chen, "Electromagnetic lens-focusing antenna enabled massive MIMO: Performance improvement and cost reduction," *IEEE Journal of Selected Areas in Signal Communication*, vol. 32, no. 6, pp. 1194–1206, Mar. 2014.

[85] A. Alkhateeb, Y.-H. Nam, J. Zhang, and R. W. Heath, "Massive MIMO combining with switches," *IEEE wireless Communications Letters*, vol. 5, no. 3, pp. 232–235, Jun. 2016.

[86] M. Mishali and Y. C. Eldar, "Blind multiband signal reconstruction: Compressed sensing for analog signals," *IEEE Transactions on Signal Processing*, vol. 57, no. 3, pp. 993–1009, Jan. 2009.

[87] R. K. R. Yarlagadda, *Analog and Digital Signals and Systems*. Springer US, 1964, p. 115.

[88] P. Feng and Y. Bresler, "Spectrum-blind minimum-rate sampling and reconstruction of multiband signals," in *Proc. IEEE International Conference on Acoustics, Speech, and Signal Processing*, Atlanta, GA, USA, May 1996, pp. 1688 – 1691.

[89] ——, "Spectrum-blind minimum-rate sampling and reconstruction of 2D multiband signals," in *International Conference on Image Processing*, Lausanne, Switzerland, Sep. 1996, pp. 701–704.

[90] R. Venkataramani and Y. Bresler, "Perfect reconstruction formulas and bounds on aliasing error in sub-nyquist nonuniform sampling of multiband signals," *IEEE Transactions on Information Theory*, vol. 48, no. 6, pp. 2173–2183, Sep. 2000.

[91] J. Chen and X. Huo, "Theoretical results on sparse representation of multiple-measurements vectors," *IEEE Transactions on Signal Processing*, vol. 54, no. 12, pp. 4634–4643, Nov. 2006.

[92] T. Tao, "An uncertainty principle for cyclic groups of prime order," *Math. Research Letter*, vol. 12, no. 1, pp. 121–127, Aug. 2003.

[93] F. Talaei, M. M. Hashemi, and S. Sadri, "Spectrum analysis and blind estimation of number of targets in multiple PRF radars based on the compressive sensing method," *IEEE Transactions on Aerospace and Electronic Systems*, vol. 50, no. 2, pp. 1004 – 1016, Jul. 2014.

[94] R. Mendez-Rial, C. Rusu, N. Gonzalez-Prelcic, A. Alkhateeb, and R. W. Heath, "Hybrid MIMO architectures for millimeter wave communications: Phase shifters or switches?" *IEEE Access*, vol. 4, pp. 247 – 267, Jan. 2016.

[95] A. Alkhateeb, Y.-H. Nam, J. Zhang, and R. W. Heath, "Massive MIMO combining with switches," *IEEE Wireless Communications Letters*, vol. 5, no. 3, pp. 232–235, Jan. 2016.

[96] S. F. Cotter, B. D. Rao, K. Engan, and K. Kreutz-Delgado, "Sparse solutions to linear inverse problems with multiple measurement vectors," *IEEE Transactions on Signal Processing*, vol. 53, no. 7, pp. 2477 – 2488, Jun. 2005.

[97] L. Liang, W. Xu, and X. Dong, "Low-complexity hybrid precoding in massive multiuser MIMO systems," *IEEE Wireless Communications Letters*, vol. 3, no. 6, pp. 653–656, Oct. 2014.

[98] D. J. Love and R. W. Heath, "limited feedback precoding for spatial multiplexing systems," in *Proc. of Global Telecommun. Conference*, San Francisco, CA, Dec. 2003, pp. 1857–1861.

[99] J. Choi, B. Mondal, and R. W. Heath, "Interpolation based unitary precoding for spatial multiplexing MIMO-OFDM with limited feedback," *IEEE Transactions on Signal Processing*, vol. 54, no. 12, pp. 4730–4740, Dec. 2006.

[100] J. Choi and R. W. Heath, "Interpolation based transmit beamforming for MIMO-OFDM with limited feedback," *IEEE Transactions on Signal Processing*, vol. 53, no. 11, pp. 4125–4135, Nov. 2005.

[101] B. Mondal and R. W. Heath, "Algorithms for quantized precoded MIMO-OFDM systems," in *Proc. IEEE Asilomar Conference on Signals, Systems, and Comp.*, Pacific Grove, CA, Nov. 2005, pp. 381–385.

[102] T. Pande, D. J. Love, and J. V. Krogmeier, "Reduced feedback MIMO-OFDM precoding and antenna selection," *IEEE Transactions on Signal Processing*, vol. 55, no. 5, pp. 2284–2293, May 2007.

[103] H. Zhang, Y. Li, V. Stolpman, and N. V. Waes, "Reduced CSI feedback approach for precoded MIMO-OFDM systems," *IEEE Transactions on Wireless Communications*, vol. 6, no. 1, pp. 55–58, Jan. 2007.

[104] K. J. Kim, M.-O. Pun, and R. A. Iltis, "QRD-based precoded MIMO-OFDM systems with reduced feedback," *IEEE Transactions on Communications*, vol. 58, no. 2, pp. 394–398, Feb. 2010.

[105] L. zhang, Z. Jin, W. Chen, and X. Zhang, "An improved adaptive channel prediction for MIMO-OFDM systems," in *Third International Conference on Communications and Networking*, China, Aug. 2008, pp. 1008–1012.

[106] C. Min, N. Chang, J. Cha, and J. Kang, "MIMO-OFDM downlink channel prediction for IEEE802.16e systems using Kalman filter," in *Proc. IEEE Wireless Communications and Networking Conference*, Kowloon, Mar. 2007, pp. 942–946.

[107] A. S. Khrwat, "Channel prediction for limited feedback precoded MIMO-OFDM systems," in *Proc. International Conference on Telecommunications*, Jounieh, Apr. 2012, pp. 1–6.

[108] D. S. Shiu, G. J. Foschini, M. J. Gans, and J. M. Kahn, "Fading correlation and its effect on the capacity of multi element antenna systems," *IEEE Transactions on Communications*, vol. 48, no. 3, pp. 502–513, Mar. 2000.

[109] T. Svantesson and A. L. Swindlehurst, "A performance bound for prediction of MIMO channels," *IEEE Transactions on Signal Processing*, vol. 54, no. 2, pp. 520–529, Feb. 2006.

[110] L. Lihong, F. Hui, Y. Tao, and B. Hu, "MIMO-OFDM wireless channel prediction by exploiting spatial-temporal correlation," *IEEE Transactions on Wireless Communications*, vol. 13, no. 1, pp. 310–319, Jan. 2014.